

# Signal Detection via Residence Times Asymmetry in Noisy Bistable Devices

A. R. Bulsara<sup>†</sup>, C. Seberino<sup>††</sup>

*Space and Naval Warfare Systems Center, Code 2363, 49590 Lassing Road, San Diego, CA 92152-6147, USA*

L. Gammaitoni<sup>\*</sup>

*Dipartimento di Fisica, Università di Perugia, Istituto Nazionale di Fisica Nucleare, and Istituto Nazionale di Fisica della Materia, Sezione di Perugia, I-06100 Perugia, Italy*

M. F. Karlsson<sup>\*\*</sup>, B. Lundqvist<sup>\*†</sup>, J.W.C. Robinson<sup>‡</sup>

*Division of Systems Technology, Swedish Defence Research Agency, SE-172 90 Stockholm, Sweden*

(November 11, 2002)

We introduce a dynamical readout description for a wide class of nonlinear dynamic sensors operating in a noisy environment. The presence of weak unknown signals is assessed via the monitoring of the residence times in the metastable attractors of the system, in the presence of a *known*, usually time-periodic, bias signal. This operational scenario can mitigate the effects of sensor noise, providing a greatly simplified readout scheme, as well as significantly reduced processing procedures. Such devices can also show a wide variety of interesting dynamical features. This scheme for quantifying the response of a nonlinear dynamic device, has been implemented in experiments involving a simple laboratory version of a fluxgate magnetometer; we present the results of the experiments and demonstrate that they match the theoretical predictions reasonably well.

05.40.+j, 02.50.Ey, 85.25.Dq

## I. INTRODUCTION

A large class of dynamic sensors have nonlinear input-output characteristics, often corresponding to a bistable potential energy function that underpins the sensor dynamics. These sensors include magnetic field sensors, e.g. the simple fluxgate sensor [1,2] and the Superconducting Quantum Interference Device (SQUID) [3], ferroelectric sensors [4], and mechanical sensors [5], e.g. acoustic transducers, made with piezoelectric materials. In many cases, the detection of a small dc or low frequency target signal is based on a spectral technique [1,2] wherein a known periodic bias signal is applied to the sensor to saturate it, driving it very rapidly between its two locally stable attractors which correspond to the minima of the potential energy function, when the attractors are fixed points. Usually, the amplitude of the bias signal is taken to be quite large, often above the deterministic switching threshold which is itself dependent on the potential barrier height and the separation of the minima, in order to render the response largely independent of the noise. In this configuration, the switching events between the stable attractors are controlled by the sig-

nal. In the presence of background noise, and absent the target signal the power spectral density of the system response contains only odd harmonics of the bias signal which we assume to be time-sinusoidal. For the case of subthreshold bias signals, one may analyse the response in the context of the *Stochastic Resonance* (SR) scenario [6] wherein the spectral amplitude of each harmonic achieves a maximum for a certain noise intensity; the threshold crossing events are noise-controlled, but a synchrony of sorts [7] between the mean crossing rate and the signal frequency is obtained for a critical noise intensity. The effect of an additional target dc signal is, then, to skew the potential, resulting in the appearance of features at even harmonics of the bias frequency  $\omega$  [8] in the system response. For the case of subthreshold bias signals, the SR scenario for this case has been analysed for prototype bistable systems [8]. The spectral amplitude at  $2\omega$  is zero unless the asymmetrizing dc signal is present, hence the appearance of power at  $2\omega$  and its subsequent analysis has been proposed as a detection/quantification tool for the target signal [8], given that  $\omega$  is known *a priori*. In practice, a feedback mechanism is frequently utilized for reading out the asymmetry-producing target signal via a nulling technique [1–3].

The above readout scheme has some drawbacks. Chief among them is the requirement of large onboard power to provide a high amplitude, high frequency bias signal for the case when one uses a suprathreshold bias signal. The feedback electronics can also be cumbersome and introduce their own noise-floor into the measurement and, finally, a high-amplitude, high-frequency bias signal often increases the noise-floor in the system. The power constraints could be mitigated somewhat by utilizing a low amplitude, low frequency bias signal, and allowing the crossing events to be largely noise-controlled; this is the SR scenario. With moderate amounts of noise, this scenario could work, the primary concern being obtaining an appreciable number of crossing events in the limited time one has to observe the target signal. Since the bias signal is controllable one could, in principle, adjust its amplitude to obtain an adequate number of crossing events per unit time, assuming that the noise floor and locations of the stable minima of the potential energy function are be-

yond control. If the crossing rate is (even approximately) known in the absence of the bias signal, then the signal frequency may be appropriately adjusted to yield optimal performance [6,8]. In some situations involving high noise intensity, one may not even need a bias signal, if the noise is strong enough to yield an acceptable crossing rate. This special case is intriguing; it affords the possibility of operating the sensor (clearly under very specific conditions) with minimal onboard power. This situation was discussed earlier [9]. Clearly, however, any sensor configuration, particularly one with a subthreshold bias signal, is very dependent on the conditions of the experiment or the particular signal analysis task at hand. The commonly used measure to describe SR, the signal-to-noise ratio at the fundamental or a higher harmonic frequency of the periodic bias signal, is not always the most informative one from a signal analysis standpoint. Rather, information-based measures [10] which can be connected to the signal detection statistics may be more useful; such a description has been rigorously obtained in the SR scenario for a prototype system subject to a small asymmetrizing dc target signal with a known time-periodic bias signal, in gaussian background noise [11].

The above preamble delivers an outline of readout schemes based on a computation of the power spectrum or information transfer as an appropriate measure of the system response. We propose here, a description of the system dynamics which makes possible the use of a measurement technique based on the system residence times in its steady states [9]. For a two-state system, the residence time in one of the stable steady states, is defined as the time elapsed between the first crossing of that threshold and the first crossing of the other threshold. In the presence of a noise background, the residence times in the stable states have random components. The residence time statistics in a bistable system were proposed for the first time in [12] as a quantifier for the SR phenomenon which involves, as already mentioned, *subthreshold* driving signals. They have also been studied in a prototype bistable model system [13]. Important features of the residence times distributions are often seen in neurophysiological experimental data; it is widely believed that the point process generated by successive “firing” events contains much relevant information about the stimulus that lead to the firing [14]. Under the appropriate conditions on the spike train, most importantly a renewal character corresponding to uncorrelated crossing events, [15] it is possible to connect the “Inter-Spike Interval Histogram” (the Residence Times Distribution, RTD, in the language of this paper) to the output power spectral density. Here we propose to use the crossing statistics [16] in order to gain information on the presence of small unknown target signals in a nonlinear dynamic detector, taken to be a two-state system for the remainder of this work.

We start by noting that absent any background noise, and with a *suprathreshold* bias signal amplitude, one obtains the same residence times in each stable state, with two crossing events per period of the bias signal. With

a small (compared to the potential barrier height) target signal, taken to be dc throughout this work, the potential is skewed at the outset of each measurement. Hence one obtains unequal residence times in the two states. The residence times can be computed analytically in some limiting cases (see below and [9]). In the presence of weak noise, having rms amplitude small compared with the bias signal, amplitude one obtains a spread in the residence times which must now be described statistically. For the case in which the bias signal is suprathreshold, the residence times distributions for the right and left potential wells will be almost symmetric with a mean value, roughly corresponding to the deterministic residence time, approaching the distribution mode. Absent the target dc signal, the distributions coincide. The presence of the external target signal, assumed very small compared to the potential barrier height, renders the potential asymmetric with a concomitant difference in the mean residence times which, to first order, should be expected to be proportional to the asymmetry-producing target signal itself. Hence, the difference between the mean residence times in the two states of the system provides an observable that can be used as a quantifier for detecting the presence of the target signal.

This procedure has some advantages compared to the conventional readout scheme: it can be implemented experimentally without complicated feedback electronics, with or without the presence of bias signals (depending on the experimental scenario, as mentioned above). In fact, the difference in residence times is quantifiable even in the *absence* of the periodic bias signal, with only noise driving the sensor between its steady states although, as outlined earlier, practical considerations e.g. observation times that depend on the relative magnitude of the noise standard deviation and the barrier height may limit the applicability of this procedure in some cases. The residence-times based technique works without the knowledge of the computationally demanding power spectral density of the system output (in most cases a simple averaging procedure on the system output works just fine) and, finally, it performs well in the presence of noise. We hasten to note that threshold statistics underpin the class of “level- crossing detectors” that have been available for a variety of applications for almost fifty years. The method outlined above has, in different forms, been used in nonlinear sensors (especially sensors that have a hysteretic output-input transfer characteristic such as those that utilize the dynamics in a ferromagnetic core in the signal detection stage), albeit without a clear understanding of the ramifications of sensor noise on the physics of the measurement [2].

The afore-described ideas are quantified in the framework of a mean field model for the evolution of the average magnetization in a ferromagnetic core. Detection of a dc target signal is achieved by pre-biasing the core with a *suprathreshold* time-periodic signal which we take to be sinusoidal, although other periodic waveforms may be better suited for specific applications; we introduce

one such waveform and compare the system response to this signal, to the response to a sinusoidal signal having the same frequency and a suitably defined equivalent amplitude. The object of the paper is to compute  $\langle \Delta T \rangle$ , the ensemble-averaged (in the presence of noise) difference in mean residence times for the right and left wells of the potential function, when a small dc signal causes an asymmetry. To lowest order,  $\langle \Delta T \rangle$  should be proportional to the target signal. Our calculations are carried out in the context of experiments on a so-called Advanced Dynamic Fluxgate Magnetometer (ADFM) prototype, a room-temperature magnetic field detector that is envisioned to use the residence times readout scheme; some preliminary experimental results, obtained with a very simple laboratory prototype, are presented in the latter sections of the paper. The dynamics of the ferromagnetic core subject to a symmetry-breaking dc target signal, together with a known bias signal in background noise are examined, the object being a computation of the difference  $\langle \Delta T \rangle$  in the residence times; however, we also recast the dynamics in terms of the more familiar standard-quartic (or Duffing) bistable potential description. This system, usually analytically more tractable than the complex dynamics that it mimics in this case, has been extensively utilized as a “test-bed” for a plethora of nonlinear stochastic dynamic phenomena, and it can be expected to yield results that are in good qualitative agreement with those from systems described by more complex (but still bistable) potential functions. Using this “equivalent” standard quartic representation, the issue of optimal achievable accuracy and bounds thereon is also addressed, using stochastic perturbation theory; a family of estimation procedures that are asymptotically optimal for vanishingly small noise is developed using this theoretical machinery. Numerical simulations have shown [18] that the estimators that are so-developed and optimized for very small noise, are also applicable to larger noise intensities.

We find that while the standard quartic yields, for the most part, the same qualitative behavior as the “soft” (so-called because it has a shallower slope at  $x \rightarrow \infty$  than the much steeper Duffing or “hard” potential) potential function that describes the “single domain” ferromagnetic sample in the mean field limit, there are some differences in the behavior predicted by the two potentials, and we highlight and explain these differences where they occur. We also invoke, where necessary, the simplest of all static threshold systems with hysteresis, the Schmidt Trigger (ST) [17] as a tool to obtain analytic results which are expected to show the same qualitative behavior as more complicated dynamical two-state systems. Finally, we note that the ideas in this paper may be extended to tri- or multi-stable dynamic systems, e.g. the class of  $(\Phi^2)^3$  models discussed by Rao and Pandit [19].

## II. MODELS AND DETERMINISTIC DYNAMICS

The best-known system that exhibits hysteresis [21], is the ferromagnet, usually described by Ising-type models [21,22], and exhibiting a phase transition to the paramagnetic state when the temperature  $T$  exceeds the Curie temperature  $T_c$ . One may describe the ferromagnet by a Landau free energy function that is even in the order parameter (the magnetization  $m$ ); this potential energy function is, then, bistable in the ferromagnetic phase, becoming monostable in the paramagnetic phase. The transition to monostability can be achieved by sweeping the temperature through the Curie point or applying an external magnetic field which breaks the symmetry of the potential, causing one of the metastable states to disappear when the field amplitude exceeds a critical value. Of course, this begs the question of having a continuum model in which one may incorporate the dynamical behavior of the ferromagnet, including the effects of time-dependent external magnetic fields. This is accomplished through mean field theory [22] which allows one to use a master equation for the *averaged* magnetization  $x(t)$  and arrive at the dynamic equation:

$$\tau \frac{dx}{dt} = -x + \tanh \left[ \frac{x + h(t)}{T} \right] \equiv -\frac{\partial U}{\partial x}(x, t), \quad (1)$$

where  $\tau$  is a system time constant, and  $T$ , a dimensionless temperature [20].  $h(t)$  is an external magnetic field that may be time-dependent, having the dimension of  $m$ . We have also expressed eq. (1) in terms of the gradient of a potential energy function (the analog of the free energy function referred to above):

$$U(x, t) = \frac{x^2}{2} - \frac{1}{c} \ln \cosh[c\{x + h(t)\}], \quad (2)$$

where we set  $c = T^{-1}$ . The potential energy function (2) is bistable for  $c > 1$ . Dynamical hysteresis in the system (1) and other systems (see below) with qualitatively similar potential energy functions, with  $h(t)$  often taken to be time-sinusoidal, has been the subject of much recent study [23,24]; cooperative phenomena, e.g. SR, arising in the presence of background fluctuations [24,25] have also been examined in the literature. The role of background fluctuations has been ignored in the derivation of (1); however, in our ensuing work, a fluctuation term will be added, phenomenologically to the rhs, in an attempt to capture the influence of the noise-floor.

The theoretical part of this paper is an attempt to make contact with laboratory experiments carried out with a crude rendition of a fluxgate magnetometer, consisting of a ferromagnetic ring core wound with a primary (input) coil and a secondary (output) coil. Details of the setup are given in section 7. We are interested in a “macroscopic” magnetic description of the fluxgate dynamics, rather than a detailed micromagnetic description

based on individual domain dynamics; a detailed derivation of mean field dynamics of the form (1) is not our intent. Rather, we use an equation of the form (1) to model the dynamics of the entire core, assuming the applicability of the mean field description. Such modeling has been used in the literature [1,2] and we will find that the model yields reasonably good (given that it is, at best, an approximation to a detailed micromagnetic description of the domain dynamics) agreement with the experimental results, thereby validating our description. Other collective approaches to the stochastic dynamics of aggregates of monodomain ferromagnetic particles do exist in the literature [26] usually starting from the Landau-Gilbert equations [27] for a single-domain particle with thermal noise included; stochastic resonance in such a system has also been studied [28].

As mentioned earlier, the model (1) will be augmented by an additive noise term; in this section, however, we will focus attention on the deterministic dynamics. In practice the time constant  $\tau$  is very important, particularly in the presence of noise. If  $\tau$  is the smallest time-scale in the system, i.e., both the noise bandwidth (defined for gaussian noise as the inverse of the correlation time  $\tau_c$ ) and the bias signal period are well within the system bandwidth  $\tau^{-1}$ , then the device essentially behaves like a static nonlinearity, with the lhs of (1) equated to zero. Hence, the dynamics are reduced to following the dynamics of the noise plus the signal, as they traverse two thresholds, given essentially by the fixed points of the potential (2). This procedure has already been described for bistable systems subject to subthreshold time-sinusoidal bias signals. It is convenient to start our description of the deterministic dynamics with this assumption and a *suprathreshold* bias signal having the form  $h(t) = A \sin \omega t$  (period  $T_0 = 2\pi/\omega$ ), since an analytic solution of the equation (1) is not possible for large bias signal amplitudes. We note that in practical devices, the bias signal is known, and controllable; hence we will assume, always, that the signal parameters can be varied at will. We also remind the reader that the bias signal plays a critical role in conventional readout schemes, via the appearance of even harmonics of the frequency  $\omega$  in the output power spectral density (PSD) of  $m$  when the symmetry-breaking target dc signal is applied [8].

In this work, we will assume the deterministic bias signal  $h(t)$  to be *suprathreshold* i.e., switching between the two stable attractors in the potential system, or between the static thresholds when the device dynamics are irrelevant, is controlled by the bias signal, with one threshold crossing occurring during each half-cycle; the exact time to threshold crossing depends, of course, on the system and bias parameters. The variable of interest for the deterministic situations of this section is, then, the difference  $\Delta T = |T_+ - T_-|$ , the difference between the residence times in the states of the two-state system. This quantity is clearly a function of the system and bias parameters. It is zero when the two stable states are symmetric about the unstable fixed point, and acquires a fi-

nite value when a dc target signal breaks this symmetry. Figure (1) demonstrates the “rocking” of the potential energy function (2) with a bias signal  $h(t) = A \sin \omega t + \varepsilon$ , ( $\omega = 2\pi/T_0$ ) when the dc offset  $\varepsilon$  is zero and also when it is finite. Of course, one could also examine the response to *subthreshold* bias signals, the “Stochastic Resonance” (SR) scenario. We will not do so in this paper, however, since a large body of literature already exists on this subject [6,8].

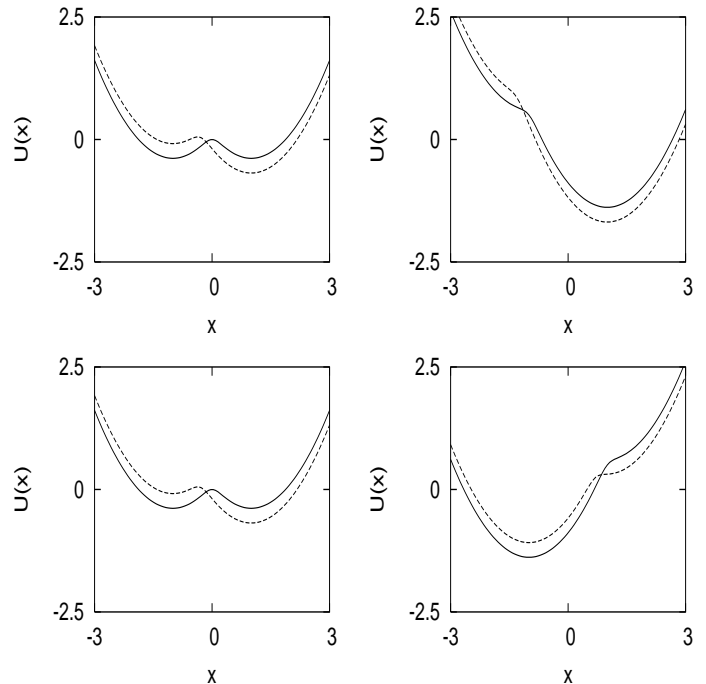


FIG. 1. Mean field potential (2) ( $c = 6$ ) with sinusoidal driving signal having amplitude  $A = 1$  and period  $T_0$ . Solid lines depict potential at times  $t = 0$  (upper left),  $T_0/4$  (upper right),  $T_0/2$  (lower left),  $3T_0/4$  (lower right). Dashed line depicts potential having additional dc offset  $\varepsilon = 0.3$

Consider first the simplest possible manifestation of a two-state system, the Schmidt Trigger (ST) [17], characterized by a two-state output and a hysteretic transfer characteristic. Its output rests in one state as long as the input voltage is less than a threshold. The switch to the other state is almost instantaneous (the ST can be modeled as the limiting case of a dynamical system [29] with very small time constant  $\tau$ ), occurring when the input voltage exceeds the threshold. Let  $\pm b$  be the ST thresholds, with  $h(t)$  the suprathreshold time-sinusoidal signal introduced above, and  $\varepsilon (\ll b)$  a dc target signal whose effect is to “displace” the sinusoidal signal upwards by an amount  $\varepsilon$ . Then, crossings of the upper and lower thresholds occur at  $h(t_{10}) + \varepsilon = b$  and  $h(t_{20}) + \varepsilon = -b$ , at times  $t_{1,20}$  respectively. Thus,

$$t_{10} = \omega^{-1} \sin^{-1} \left( \frac{b - \varepsilon}{A} \right); \quad t_{20} = \omega^{-1} \left[ \sin^{-1} \left( \frac{b + \varepsilon}{A} \right) + \pi \right]. \quad (3)$$

The next up-crossing occurs at  $t_{30} = t_{10} + 2\pi/\omega$ , since  $h(t)$  is suprathreshold and one can expect an up (or down)-crossing within every half-cycle of the signal. Then  $T_+ = t_{20} - t_{10}$  and  $T_- = t_{30} - t_{20}$ , whence we obtain,

$$\Delta T_{ST0} = 2\omega^{-1} \left[ \sin^{-1} \left( \frac{b + \varepsilon}{A} \right) - \sin^{-1} \left( \frac{b - \varepsilon}{A} \right) \right]. \quad (4)$$

Defining a "sensitivity" via  $S(\varepsilon) = \frac{d\Delta T}{d\varepsilon}$  we obtain

$$S(\varepsilon) = \frac{2}{\omega A} \left[ \left( 1 - \left( \frac{b + \varepsilon}{A} \right)^2 \right)^{-1/2} + \left( 1 - \left( \frac{b - \varepsilon}{A} \right)^2 \right)^{-1/2} \right] \quad (5)$$

which clearly increases with  $\varepsilon$ , saturating at  $\bar{\varepsilon} = A - b$ . It is instructive to note that  $\Delta T_{ST0}$  vanishes when  $\varepsilon = 0$ , and  $\Delta T_{ST0} \rightarrow \frac{4\varepsilon}{A\omega}$  for large (compared to the threshold location)  $A$ . In the large  $A$  regime, we can also show that the residence time  $T_+ \rightarrow \frac{1}{\omega} \left( \pi + \frac{2\varepsilon}{A} \right)$ , which approaches  $T_0/2$  at very large  $A$  as expected. A completely analogous set of limiting values exist for the other residence time  $T_-$ .

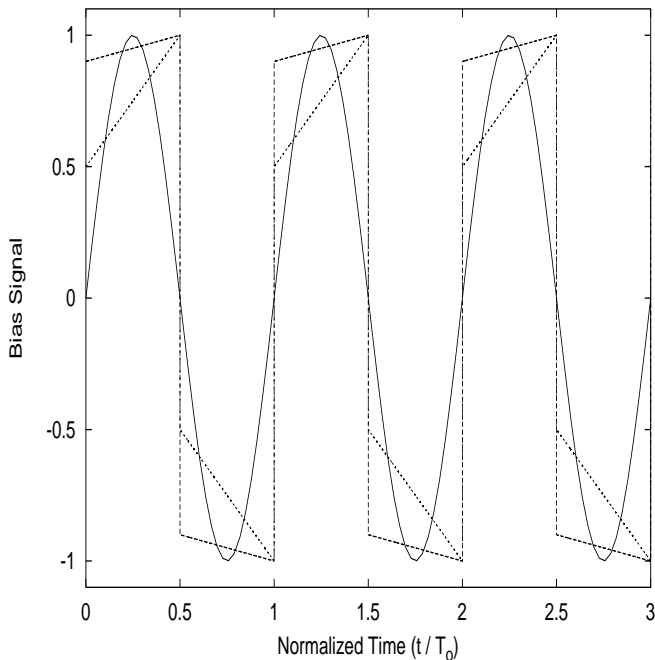


FIG. 2. Sinusoidal signal  $A \sin(2\pi t/T_0)$  with  $A = 1$ , period  $T_0 = 100$ , and two realizations of the waveform (6) obtained via (6).  $\kappa_1 + \kappa_2 = A$ , and  $\kappa_2 = 0.05$  (top waveform),  $\kappa_2 = 0.25$  (bottom waveform).

One may show that other (non-sinusoidal) bias waveforms can lead to enhanced sensitivity under the appropriate operational conditions. One such waveform is obtained by adding a square wave having amplitude  $\kappa_1$  with a triangular wave of amplitude  $\kappa_2$ , both having frequency  $\omega$ . The amplitudes of the component signals are set according to the prescription  $\kappa_1 + \kappa_2 = A$ . The result is a periodic waveform (period  $T = 2\pi/\omega$ ) given by:

$$H(t) = \kappa_1 + \frac{2\omega}{\pi} \left( t - \frac{1}{2} \frac{\pi}{\omega} \right) \kappa_2, \quad 0 < t < \frac{\pi}{\omega} \\ = -\kappa_1 - \frac{2\omega}{\pi} \left( t - \frac{3}{2} \frac{\pi}{\omega} \right) \kappa_2, \quad \frac{\pi}{\omega} < t < \frac{2\pi}{\omega}. \quad (6)$$

Figure (2) shows a sinusoidal signal having period  $T_0 = 100$  and the waveform (6) having the same period. For the waveform (6), it is clear that the parameters  $\kappa_{1,2}$  determine whether threshold crossings occur on the signal segments having slope  $\Gamma = \infty$ ,  $\Gamma < 0$ , or  $\Gamma > 0$ . In fact, it is evident that for crossings of the upper threshold, at time  $t_{10}^{(i)}$ , one has  $t_{10}^{(i)} = 0$  if  $\kappa_1 - \kappa_2 \geq b - \varepsilon$  with crossings occurring on the  $\Gamma = \infty$  segment, and  $t_{10}^{(i)} > 0$  for  $\kappa_1 - \kappa_2 < b - \varepsilon$ , for crossings occur on the  $\Gamma > 0$  segment. For the lower threshold, the crossing times are  $t_{20}^{(i)} = \pi/\omega$  for  $\kappa_1 - \kappa_2 \geq b + \varepsilon$  corresponding to crossings on the  $\Gamma = \infty$  segment, and  $t_{20}^{(i)} > \pi/\omega$  for  $\kappa_1 - \kappa_2 < b + \varepsilon$ , corresponding to crossings on the  $\Gamma < 0$  segment.

For the cases when the threshold crossings occur on the  $\Gamma \neq \infty$  segments one can, analogous to the time-sinusoidal case, obtain the upper and lower threshold crossing times as

$$t_{10}^{(i)} = \frac{b - \varepsilon - \kappa_1 + \kappa_2}{\kappa_2} \frac{\pi}{2\omega}, \\ t_{20}^{(i)} = \frac{b + \varepsilon - \kappa_1 + 3\kappa_2}{\kappa_2} \frac{\pi}{2\omega}, \quad (7)$$

whence we obtain,

$$\Delta T^{(i)} = T_0 \frac{\varepsilon}{\kappa_2}, \quad \kappa_1 - \kappa_2 < b - \varepsilon, \\ \Delta T^{(i)} = T_0 \frac{b + \varepsilon - \kappa_1 + \kappa_2}{2\kappa_2}, \quad b - \varepsilon \leq \kappa_1 - \kappa_2 \leq b + \varepsilon, \\ \Delta T^{(i)} = 0, \quad \kappa_1 - \kappa_2 > b + \varepsilon, \quad (8)$$

and the sensitivity  $S^{(i)} = \frac{\partial \Delta T^{(i)}}{\partial \varepsilon}$  is obtained as  $S^{(i)} = T_0/\kappa_2$ ,  $S^{(i)} = T_0/2\kappa_2$ , and  $S^{(i)} = 0$  for each of the three regimes defined in (8). Throughout this paper we use the superscript  $(i)$  to denote quantities (e.g. crossing and residence times) associated with the bias waveform (6).

Plotting the quantity  $\Delta T_{ST0}$  vs.  $\varepsilon$  for the two bias signal waveforms considered, shows immediately that the bias signal waveform (6) can yield a better separation  $\Delta T$  for low values of the target signal. This will be illustrated via simulations in section 4.

Finally, we introduce an alternative realization of the dynamics (1) in terms of the simpler (from an analytic standpoint) Duffing or "hard" potential:

$$\frac{dx}{dt} = -\frac{\partial U_d(x,t)}{\partial x}, \quad (9)$$

with the potential function defined as

$$U_d(x,t) = -\frac{a}{2}x^2 + \frac{b}{4}x^4 - (\varepsilon + h(t))x, \quad (10)$$

$a, b$  being constants to be determined. In the absence of any external signals ( $\varepsilon, h(t) = 0$ ) this potential has an unstable maximum at 0, and stable minima at  $x_{dp0} = \sqrt{\frac{a}{b}} = -x_{dm0}$ , with the height of the potential barrier given by  $\Delta U_{d0} = \frac{a^2}{4b}$ . For the “soft” potential (2) the corresponding quantities may readily be obtained via expansion about the limiting values for large  $c$ . We then obtain an unstable maximum at 0, with minima at  $x_{p0} = 1 + \Delta_p = -x_{m0}$ ,  $\Delta_p = (\tanh c - 1)/(1 - c \operatorname{sech}^2 c)$ . The barrier height is  $\Delta U_{p0} = \left| \frac{x_{p0}^2}{2} - \frac{1}{c} \ln \cosh cx_{p0} \right|$ . We then set the parameters  $a, b$  in (10) by demanding that the extrema, and hence the energy barrier heights, of the potentials (2) and (10) coincide when  $\varepsilon = h(t) = 0$ . This readily leads to the “equivalent” hard potential (10) with the definitions

$$a = \frac{4\Delta U_{p0}}{x_{p0}^2}, \quad b = \frac{a}{x_{p0}^2}. \quad (11)$$

The two potentials now have the same extrema and barrier height in the signal-free case; of course their slopes (for  $x \rightarrow \pm\infty$ ), are quite different. This difference leads to changes that are quantitative only, when we examine the response of both models to the target signal in the presence of a noise floor and the periodic bias signal. Hence, with the definitions (11), the hard potential affords a model that captures most of the essential physics of this class of devices; this is particularly convenient from the standpoint of analytic calculations, plus it allows us to draw on the huge body of literature on various aspects of the noisy nonlinear dynamics of these devices. We note that the energy barrier separating the stable steady states, decreases with decreasing  $c$ . For  $c < 1$ , the parabolic term in the potential (2) starts to dominate, and the dynamics approaches linearity. The case of very small energy barrier is relevant when one considers, for example, “soft” ferromagnetic cores in which one observes frequency-dependent hysteresis loop areas, as well as cores that are approximately “single domain” [30]; in these cores, the hysteresis loop is very narrow, the energy barrier is very small, and they can be well-approximated by the potential (2) with  $c \approx 1$ .

Consider now, the inclusion of a small (with respect to the barrier height) asymmetrizing dc signal  $\varepsilon$ , together with a known bias signal  $h(t) = A \sin \omega t$  that we take to be *suprathreshold*. The hard potential (10) develops points of inflexion at  $x_{fdp} = \sqrt{\frac{a}{3b}} = -x_{fdm}$ , and the threshold crossings occur when  $\varepsilon + h(t) = -ax_{fdp} + bx_{fdp}^3$  with a similar condition involving the other inflexion point  $x_{fdm}$ . The rhs of this expression is  $-x_c \equiv -\sqrt{\frac{4a^3}{27b}}$

with the opposite (i.e. plus) sign corresponding to a crossing of the inflexion point  $x_{fdm}$ . It is important to note that we are assuming the bias amplitude to be large enough that the signal dominates the dynamics so that the Duffing dynamics (9) can be approximated by the simple threshold dynamics of the form considered in the ST description, above; the crossing “thresholds” are, thus, given by the points of inflexion. In a procedure completely analogous to that utilized in the ST, we obtain the difference in residence times for the equivalent system (9) in the absence of noise:

$$\Delta T_{d0} = \frac{2}{\omega} \left| \sin^{-1} \left( \frac{x_c + \varepsilon}{A} \right) - \sin^{-1} \left( \frac{x_c - \varepsilon}{A} \right) \right|. \quad (12)$$

An analogous expression for the residence times difference may be obtained for the mean-field dynamics (1) under the same conditions, i.e assuming the system and signal parameters to be such that the system may be well-approximated by a static threshold device. The points of inflexion are at  $x_{fsp} = \sqrt{\frac{c-1}{c}} = -x_{fsm}$  and we obtain for the difference in residence times,

$$\Delta T_s = \frac{2}{\omega} \left| \sin^{-1} g_p - \sin^{-1} g_m \right|, \quad (13)$$

where  $g_{m,p} \equiv \{c^{-1} \tanh^{-1} x_{fsm,p} - x_{fsm,p} - \varepsilon\}/A$ . Analogous expressions for the waveform (6) may be derived analytically; we defer these calculations for a later section.

In the following sections we compute and analyse the mean residence times difference in the presence of system noise. As mentioned earlier, we expect the expressions (4), (12), and (13) to provide good approximations to the mean residence times difference when the known bias signal is well suprathreshold and the noise and target signal are small. Throughout this work, we will consider the  $c > 1$  case, corresponding to bistability in the potential function (2). It is worth noting, however, that temperature fluctuations (that can reasonably be expected to occur in applications) lead directly to fluctuations in the barrier height and the locations of the minima, since these quantities depend on the parameter  $c$ . Hence, we may encounter situations wherein the potential switches between mono- and bistability on the time-scale of the fluctuations. This scenario is not treated here, rather it will be addressed in a forthcoming publication.

It is very important to reiterate that the results of this paper hold true for a very large class of dynamical systems, those whose dynamics are underpinned by a bistable (or even multistable) potential energy function. The expressions for the deterministic residence times difference,  $\Delta T$ , can be analytically derived only when we ignore the (internal) system dynamics invoking the large  $A$  limit, wherein we can simply approximate the bistable dynamics by a (non-dynamic) Schmidt trigger with appropriately computed threshold settings. We now make the (deterministic) treatment of this section more realistic, by introducing a noise-floor.

### III. LEVEL CROSSING DYNAMICS IN THE PRESENCE OF A NOISE-FLOOR

We have noted that in the absence of the target signal ( $\varepsilon = 0$ ) and for the noiseless case, the bias signal periodically “rocks” the potential (figure 1). If the signal amplitude  $A$  exceeds the deterministic switching threshold, the state-point will make, successively, transitions to the two stable states at deterministic (well-defined) times separated by a half-cycle of the bias signal; these switch events are quite regular.

Now consider the noisy case; throughout this work we will assume that the noise is gaussian and correlated, i.e., it is derived from a white-noise driven Ornstein-Uhlenbeck process [31]:

$$\dot{\zeta}(t) = -\tau_c^{-1}\zeta + \sigma F(t) \quad (14)$$

where  $F(t)$  is a white noise process having zero mean and unit variance:  $\langle F(t) \rangle = 0$ , and  $\langle F(t)F(t') \rangle = \delta(t - t')$ . We readily obtain for the correlation function of the colored gaussian noise,  $\langle \zeta(t)\zeta(t') \rangle = \langle \zeta^2 \rangle \exp[-|t - t'|/\tau_c]$  where  $\langle \zeta^2 \rangle = \sigma^2\tau_c/2$ . We also assume that the signal frequency  $\omega$  is well within the noise band, i.e. the noise is wideband *vis-a-vis* the signal. This is a reasonable assumption, and it will become evident that it may be possible to somewhat mitigate problems arising from the noise statistics by adaptively adjusting the bias signal amplitude (*vis-a-vis* the noise floor and barrier height) in real scenarios.

For  $\varepsilon = 0$  and  $A$  suprathreshold (this is well represented by the condition  $\frac{Ax_0}{\Delta U} > 3/2$  where  $x_0$  denotes the location of a stable fixed point of the potential), the threshold crossings to the stable states are controlled by the signal, but the noise does introduce some randomness into the inter-spike intervals. The result is a distribution of residence times (the RTD) whose variance increases with increasing noise intensity. For  $A$  far above the deterministic switching threshold and moderate noise, the RTD assumes a symmetric narrow (almost gaussian) shape with a mean value (the mean crossing time) nearly the same as the most probable value or mode. The mean values (or modes, in this case) of the histograms corresponding to transitions to the left and right stable states coincide. As the signal amplitude decreases, the RTD starts to develop a tail so that the mean and mode get separated; the appearance of the tail is an indication of the growing role of noise in producing switching events, although the suprathreshold signal is still the dominant mechanism. When the signal amplitude falls below the deterministic crossing threshold, the crossings are driven largely by the noise. The RTD can assume a characteristic multi-peaked structure [13,32] that shows “skipping” behavior since the noise can actually cause the crossings to occur at different multiples  $nT_0/2$  ( $n$  odd) of the half-period, and the Stochastic Resonance scenario comes into play [6] through a synchronization of characteristic time-scales in the system; the noise determines

the tail of the RTD, and introduces a (symmetric) broadening, or dispersion, in individual lobes of the RTD, since the individual crossing events do not always occur precisely at times  $nT_0/2$ . We will not consider this (so-called *subthreshold*) case in the current paper, limiting ourselves to the *suprathreshold* bias signal case only.

We re-iterate that with zero target signal, the crossing statistics to the left or right minimum of the potential, are identical, with coincident RTDs, as should be expected. However, let us now consider the case of a nonzero but small target signal,  $\varepsilon x_0 \ll \Delta U_{p0}$ , that is sufficient to skew the potential (figure 1) but not remove one of the minima, in the presence of gaussian noise and the bias signal  $A \sin \omega t$ . Before presenting simulation results, we comment on some features that we should expect to observe in the RTDs:

1. The potentials (2) and (10) are now *a priori* skewed even for  $A = 0$ . Hence, the mean residence times in the two stable states will be different. Denote these times by the ensemble-averaged quantities  $\langle T_+ \rangle$ ,  $\langle T_- \rangle$  respectively.

2. For very large bias signal amplitudes and moderate noise intensity ( $\sigma^2 \leq \Delta U_{p0}, \Delta U_{d0}$ ), the RTDs are two well-separated symmetric near-gaussian distributions centered about modes that coincide with their means  $\langle T_{\pm} \rangle$ ; for signal amplitudes much larger than the rms noise amplitude, the distributions tend to coincide. As the noise intensity increases the distributions become broader and, as the bias signal amplitude drops to the deterministic switching threshold and below, start to develop tails with separated modes and means.

3. The separation  $\langle \Delta T \rangle = | \langle T_+ \rangle - \langle T_- \rangle |$  of the mean values yields a direct measure of the asymmetry-producing target signal. It can be calculated for the zero noise case (section 2), as well as with weak noise and bias signal amplitude  $A$  that is well-suprathreshold. We will find in fact (section 5) that, in the large  $A/\sigma$  limit,  $\langle \Delta T \rangle$  is well-approximated by its deterministic analog, and is proportional to the asymmetrizing signal  $\varepsilon$ . Theoretical calculations of this quantity are currently underway, but numerical simulations are shown below. For an *a priori* balanced device (i.e. symmetric potential function), in fact, the existence of a non-zero  $\langle \Delta T \rangle$  can be taken as a sign of the presence of the target signal.

4. In the presence of increasing amounts of noise the RTDs tend to merge and their mean values (which are now well-separated from the modes) also may be difficult to distinguish, since  $\langle \Delta T \rangle \rightarrow 0$  with increasing noise. However, increasing the bias signal amplitude (this could be done adaptively in a real application) once again leads to the signal as the dominant mechanism for crossing events and the distributions “sharpen” somewhat and have less overlap, becoming more resolvable, even though the separation  $\langle \Delta T \rangle$  may actually decrease.

5. For *subthreshold* bias signals, the crossing events are noise-dominated and the RTDs multimodal in general. The Stochastic Resonance [6] scenario may be exploited

to yield better signal processing. This scenario has been extensively discussed in the literature; we do not dwell on it here.

6. For very special situations, primarily those in which there is a small amount of noise, one can carry out the above procedure with a very weak bias signal. In this case the RTDs for each potential well are almost unimodal with long tails. The mean values and modes are, again, dependent on the target signal; however, in this case, the slopes of the long-time tails of the density functions are different for the two wells, and this difference can also be used as an identifier, if needed, of the target signal. The limiting case of zero bias signal has also been studied [9]; our studies indicate that this operating mode may be optimal even for small target signals  $\varepsilon$ , with  $\langle \Delta T \rangle$  proportional to  $\varepsilon$ . This operating mode relies on the presence of background noise that is strong enough to initiate inter-well switching events without the presence of a suprathreshold bias signal. Of course, in practical applications, the presence of assorted (often non-Gaussian and non-stationary) noise sources, as well as readout issues, could make the zero bias signal mode a possibility for only very specialized scenarios. For these, more complicated, noise backgrounds, the renewal assumption for the crossing events cannot be expected to hold. This operation mode may be particularly well-suited for applications wherein the potential barrier height can be adjusted during an experiment. It does afford the attractive possibility of significantly reduced onboard power.

7. Our calculations to date indicate that a sinusoidal bias signal is not always optimal; in some operational scenarios, better sensitivity may be obtained, by using other signal waveforms, e.g. the waveform (6) or a triangular waveform, which have a stepwise linear behavior. An exhaustive study along these lines is beyond the scope of this paper, however, we do present results (next section) based on a bias signal of the form (6). In general, however, the choice of optimal bias waveform is very dependent on the system and signal parameters in a given operating scenario.

Note that in an experiment, under any of the above scenarios, it is *not* necessary to actually compute the RTDs. One simply accumulates crossing times for the two saturation states of the hysteresis loop, and computes the arithmetic mean for each set of residence times. Then, an important issue is the amount of data (dependent on the response time of the electronics), the amount of time one can “look” at the target signal, as well as the bias frequency  $\omega$  required to obtain reliable estimates of  $\langle \Delta T \rangle$ . It is clear that increasing the bias signal amplitude, in order to better-discriminate the RTDs, can lead to enhanced detection probabilities. In this context, it is important to point out that the above technique may be implemented with bias signal amplitudes that are not substantively larger than the potential barrier height, and also with relatively low bias frequencies; this is true particularly for the new “single-domain” [30] class of magnetic fluxgate sensors which have mainly gaussian

correlated noise and small  $1/f$  risers. In practice, however, one should expect to confront a tradeoff between the bias signal amplitude (this is a function of the on-board power in a practical sensor) and the concomitant degree of resolution of the peaks of the histograms, and what is necessary for a reliable estimate, usually with a limited observation time, of the target signal from  $\langle \Delta T \rangle$ .

#### IV. SIMULATIONS

We now show the results of numerical simulations carried out on the original mean-field model (1) as well as the equivalent quartic model (9), using a sinusoidal bias signal as well as the waveform (6), with a gaussian noise background present in all cases. The noise is assumed to enter additively on the rhs of both models. We use  $c = 4$  for all simulations; this completely defines both (bistable) potentials via (2) and (10). The value of  $c$  remains constant throughout this work, it being assumed that this parameter cannot easily be adjusted in experiments. Note that real devices usually have a time-constant  $\tau$ , that sets the device bandwidth. The time constant  $\tau$  of real devices, is usually about  $10^{-8}$  so that, in the simulations, the signal frequency and noise band are all adjusted to lie well within the instrument bandwidth  $\tau^{-1}$ . For theoretical calculations, this implies that one may represent the device as a “static” nonlinearity, analogous to our approach in section 2, and simply track the noise and signal dynamics as they pass through the system. Under these conditions, the results for different signal frequencies (as long as  $\frac{\omega}{2\pi} \ll \tau^{-1}$ ) are very similar; for frequencies larger than  $\tau^{-1}$ , however, dynamic hysteresis effects can become more important. In our simulations, we consider a dynamical device wherein the time-derivative term cannot simply be discarded; we take  $\tau = 1$ . Finally, we set the correlation time of the noise as  $\tau_c = 0.1$  and the bias signal period  $T_0 = 100$ , so that the bias signal is within the noise-band. In this work, we do not investigate the effects of noise color, the subject of a huge amount of attention in the literature (see e.g. [33]); this analysis is deferred to a later publication.

The results of simulations, wherein we examine the effects of changing the noise variance  $\sigma^2$ , the bias amplitude  $A$ , and the (dc) target signal  $\varepsilon$ , are shown in figures (3) and (4). In both cases, the top row shows the probability density of residence times computed using a sinusoidal bias signal (left panel) and the waveform (6) (right panel), as a function of the normalized time  $t/T_0$ . Results are shown only for the mean field model (1), in the interests of clarity; in all cases, however, we obtain excellent agreement when the simulations are carried out using the equivalent quartic model (10), with parameters computed via (11). The bottom row of each figure shows the residence times difference  $\langle \Delta T \rangle$  as a function of the noise variance  $\sigma^2$ . The bias amplitude  $A$  is suprathreshold in all cases; we remind the reader that

the case of zero bias signal has already been discussed in [9], and the case of subthreshold bias signal (the SR scenario) has also been extensively discussed in the literature; we do not address these situations here. The following features are observed:

1. Increasing the noise variance, leads to an increase in the standard deviation of the density function; the two components of the RTDs broaden and, simultaneously, lose height at their modes so that the normalization is preserved. As the bias amplitude  $A$  approaches the deterministic switching threshold, one expects the noise to play an increasingly important role in switching events; this would lead to a tail in the density function, and a separation of the mean value, from the mode. In all cases, the distributions remain symmetric about  $T_0/2$ , as expected.

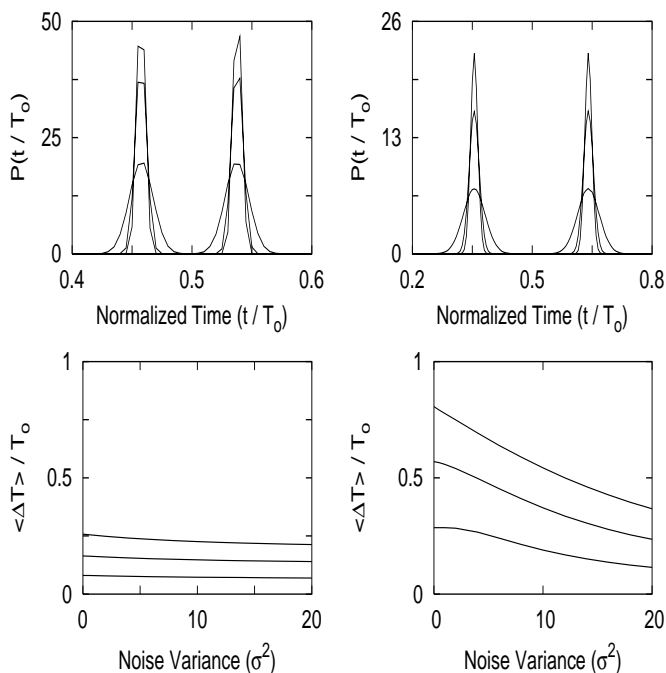


FIG. 3. Residence times density vs. normalized time for noise variance parameters  $\sigma^2 = 0.05, 0.1, 1.0$  (top to bottom) for mean field model ( $c = 4$ ) with bias signal of amplitude  $A = 1.0$  and period  $T_0 = 100$ , and asymmetrizing dc signal  $\epsilon = 0.1$ . Left panel: sinusoidal driving signal. Right panel: waveform (6) with  $\kappa_1 + \kappa_2 = A$ ,  $\kappa_1 = 2\kappa_2$  (note the different scale). Lower panels: mean residence times difference vs.  $\sigma^2$  for changing target dc signal.  $\epsilon = 0.3$  (top),  $0.2$  (middle), and  $0.1$  (bottom).

2. The waveform (6) leads to a larger separation of the mean values, particularly at low to intermediate noise intensities (see lower panels). Hence, it may be more convenient to use this bias waveform for specific operational situations, wherein resolution is a problem and signal observation times are constrained.

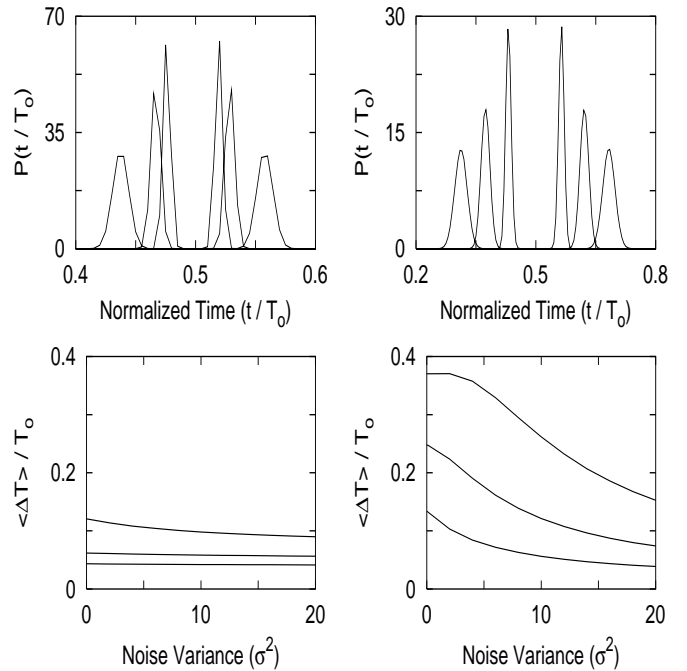


FIG. 4. Same as figure 3 with noise variance parameter  $\sigma^2 = 0.1$ ,  $\epsilon = 0.1$ , and bias amplitude  $A = 1.6$  (tallest pair),  $1.2$  (middle pair), and  $0.8$  (lowest pair). Curves in lower panels correspond to  $A = 0.8$  (top),  $1.2$  (middle), and  $1.6$  (bottom).

3. While the sinusoidal bias signal clearly has a fixed waveform (specified by its amplitude and frequency), the waveform (6) can be adjusted by choosing the relative values of  $\kappa_1$  and  $\kappa_2$ , subject to the constraint  $\kappa_1 + \kappa_2 = A$ . Hence, it is worth the digression, at this point, to investigate the value of  $\langle \Delta T \rangle$  as a function of the parameters  $\kappa_1$  and  $\kappa_2$  in (6). In order to compare this value with the value obtained for the sinusoidal bias signal we keep the condition  $\kappa_1 + \kappa_2 = A$ . In fig. (5) we show  $\langle \Delta T \rangle$  as a function of  $\kappa_2$  for different values of the noise intensity together with the value obtained for the sinusoid. The dynamical system described by the “soft” potential (2) is simulated, so that only one (internal) adjustable parameter  $c$ , changes the shape of the potential. The data points represent the theoretical prediction obtained by approximating the double well potential with the “equivalent” (see section 2) Schmidt trigger system:

$$\begin{aligned}
 \langle \Delta T \rangle &= 0, \quad \kappa_2 < \frac{1}{2}(A - b - \epsilon) \\
 \langle \Delta T \rangle &= \frac{2\pi b + \epsilon - A + 2\kappa_2}{\omega 2\kappa_2}, \\
 \frac{1}{2}(A - b - \epsilon) &\leq \kappa_2 \leq \frac{1}{2}(A - b + \epsilon) \\
 \langle \Delta T \rangle &= \frac{2\pi \epsilon}{\omega \kappa_2}, \quad \kappa_2 > \frac{1}{2}(A - b + \epsilon), \quad (15)
 \end{aligned}$$

where we have re-arranged the result in (8), and set the threshold  $b$  as in (13). The non-monotonic behaviour of

$\langle \Delta T \rangle$  as a function of  $\kappa_2$  can be readily understood by using the same argument presented for the derivation of (8). It is interesting to note that there exists an optimum value for  $\kappa_2$  and that by a proper selection of the combination  $\kappa_1, \kappa_2$  the waveform in (6) can outperform (in terms of  $\langle \Delta T \rangle$ ) the more conventional sinusoidal bias; in fact, one observes that  $\kappa_2 = A$  (a purely triangular bias signal) most closely approximates the sinusoidal waveform. The values of  $\langle \Delta T \rangle$  for the sinusoidal bias signal with the noise intensities used in the figure, are very close (indistinguishable on the scale of the figure) to the horizontal line (corresponding to the deterministic case); this is to be expected since the curves generated using the waveform (6) also converge to the same value at large  $\kappa_2$ . With decreasing noise intensity, the curves approach the deterministic case (the large  $A/\sigma$  limit), and the optimal  $\kappa_2$  is then given by  $\kappa_{2c} \approx (A - b - \varepsilon)/2$ . The effect of changing  $c$ , while keeping all the driving parameters fixed, is to change the barrier height and the separation of the potential minima. For decreasing  $c$ , the barrier height decreases, the curves in figure (5) tend to converge towards the deterministic results, i.e. the zero noise case, more rapidly; in addition, the optimal value of  $\kappa_2$  moves towards lower values and the maximal separation  $\langle \Delta T \rangle$ , at the optimal  $\kappa_2$ , is lower.

4. At very large noise,  $\langle \Delta T \rangle$  approaches zero. This is expected, with the distributions overlapping more and more with increasing noise. The approach to zero is slower for larger target signals because of the larger asymmetry in the potential that they bring. Also, the details about the potential and the bias signal waveform, become increasingly irrelevant as  $\sigma^2$  increases.

5. At vanishingly small noises,  $\langle \Delta T \rangle$  is almost flat, for small target signals, and shows a monotonic decrease with increasing noise. At zero noise (not shown on the plots) the curves would intersect the vertical axis at the deterministic difference  $\Delta T$ .

6. Increasing the bias signal amplitude reduces  $\langle \Delta T \rangle$  even as it renders the distributions somewhat more resolvable for large noise (see figure (4)). This indicates that in a practical application, it may not necessarily be of benefit to apply an extremely large bias signal (see the next section); our simulations show that bias signals having amplitude not much larger than the barrier height will suffice. Of course, exceptional cases e.g., large noise, or non-gaussian and/or non-stationary noise, may necessitate the application of larger drive signals. An important point to be made here is that the (possibly detrimental) effects of a large noise background may be reduced – but not entirely eliminated – by carefully increasing the bias signal; this procedure can also render the device response somewhat immune to the noise statistics. Such an “adaptive” control could be achieved by, e.g., a neural network in practical situations. Using the waveform (6) leads (see figure (4)) to a somewhat cleaner resolution of the modes of the RTDs with increasing bias amplitude, and, as already noted, the difference in mean residence times is actually greater than in the sinusoidal driving case, with

the appropriate selection of  $\kappa_2$ . The fact that the waveform (6) is locally *linear* where the threshold crossings occur, contributes to the far better resolution of the residence times difference  $\langle \Delta T \rangle$  that it brings. In all cases, a very large bias signal has the effect of effectively linearizing the response, with the residence times densities merging into a single peak centered at  $T_0/2$ .

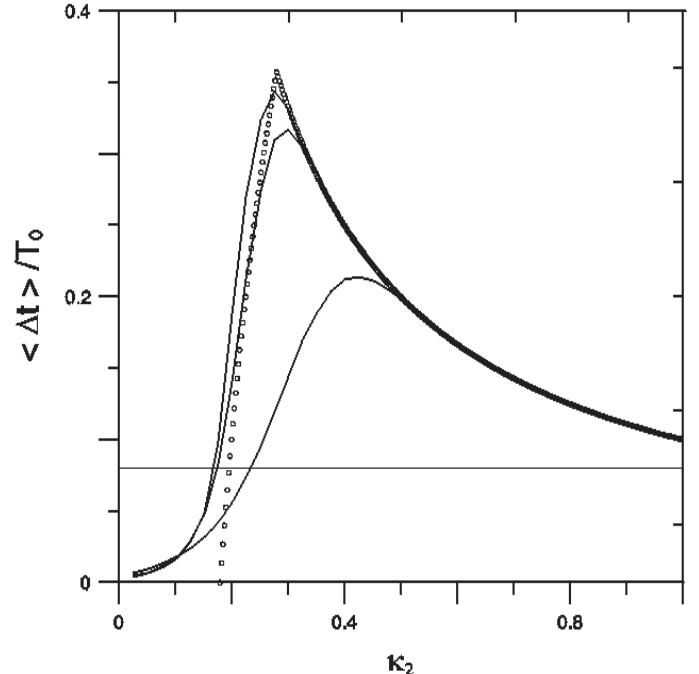


FIG. 5. Effect of varying parameters in the *suprathreshold* bias waveform (6). Normalized mean residence time difference vs.  $\kappa_2$  for dynamical system described by (1) and (2).  $c = 4$ ,  $A = 1$ ,  $\kappa_1 + \kappa_2 = A$ ,  $T_0 = 100$ ,  $\varepsilon = 0.1$ . Solid curves correspond (left-to-right) to noise intensity  $\sigma^2 = 0, 1.0, 10.0$ . Dotted curve denotes result obtained via “equivalent” deterministic ( $\sigma^2 = 0$ ) threshold model (15). Horizontal line denotes  $\Delta T$  for sinusoidal bias waveform with same amplitude and frequency, and zero noise; lines corresponding to different noise intensities (for sinusoidal driving case) are indistinguishable from deterministic case on scale of the figure.

7. In the limit of low noise and suprathreshold bias amplitude one expects the simple “non-dynamical” picture presented in section 2, to yield a very good description of the dynamics, with the mean residence times well approximated by the deterministic expressions (12) and (13). A simple calculation in the next section, will demonstrate this point nicely. From a practical standpoint, the fact that one can, in the low-noise case, compute *a priori* the expected observable  $\langle \Delta T \rangle$  via the deterministic quantity for given target and bias signals, can be of considerable utility in practical applications.

8. The difference in means  $\langle \Delta T \rangle$  is proportional to the target signal, provided the latter is weak [9]. The smallest target signal strength ( $\varepsilon = 0.1$ ), used in the

figures is relatively strong so that this relationship may be only approximately true, with higher order terms (in  $\varepsilon$ ) giving a non-vanishing contribution to  $\langle \Delta T \rangle$ .

9. As already noted, but not shown in the figures, the two descriptions (mean field and equivalent quartic) give very similar results, with some quantitative differences attributable to the approximation (11), wherein the mean field potential is replaced by a “harder” potential (the quartic model). The relevant observable  $\langle \Delta T \rangle$  is virtually identical for both models except for some minor differences, partly attributable to simulation difficulties, at very low noise intensities.

Finally, we comment here on an interesting effect, *Resonant Trapping* (RT) [34], which is observed when the bias signal amplitude is just barely above the deterministic switching threshold. In this regime, the noise can actually cause the system to miss a threshold crossing; the state point remains trapped in one of the stable attractors (or near the unstable point of the potential) by the noise. This effect leads [9] to a maximum in  $\langle \Delta T \rangle$  at a critical noise intensity; the effect (which should *not* be confused with the substance of figure (5)) disappears as the bias signal amplitude is increased, to the point where the crossings are, predominantly, driven by the signal. Clearly, RT is a mechanism that affords the possibility of using even weaker bias signals - usually desirable because of power constraints - while exploiting the intrinsic noise floor of the device. A very detailed study of RT in this class of systems will be published in a forthcoming paper.

In the following section, we present an attempt to characterize performance via a signal-to-noise ratio (SNR) which we may compute analytically in the limit of small noise, by asymptotic expansions. We also comment on the notion of a finite observation time  $T_{ob}$ .

## V. TOWARDS PERFORMANCE OPTIMIZATION

Following the results of the preceding section, one may ask the logical question: what is the optimal detector configuration for the detection of a given target signal in a noise background? As discussed in earlier work [9], the (theoretical) largest  $\langle \Delta T \rangle$  is obtained for zero bias signal. However, in real applications this observation must be tempered by the constraint of finite observation time  $T_{ob}$ . The noise intensity should be high enough to allow switching events so that the system yields acceptable sensitivity and SNR without the bias signal. Otherwise, a bias signal must be applied. In the following we introduce a quantifier to take into account both the  $\Delta T$  amplitude and the observation time  $T_{ob}$  and discuss the optimal bias signal for given target amplitude, background noise intensity, and potential barrier height.

We start by assuming that we have collected  $N$  samples for each of the residence times  $T_{n\pm}$ . The mean values of the two RTDs are  $\langle T_{n\pm} \rangle$ ; as discussed above, these may be computed directly from the crossing times data

sets (the subscript  $n$  denotes an experimental or simulated quantity). The actual mean values  $\langle T_{\pm} \rangle$  are then given by,

$$\langle T_{\pm} \rangle = \langle T_{n\pm} \rangle + \langle \delta T_{n\pm} \rangle, \quad \langle \delta T_{n\pm} \rangle = \frac{\sigma_{T_{n\pm}}}{\sqrt{N}}, \quad (16)$$

where  $\sigma_{T_{n\pm}}$  is the standard deviation of each distribution. The second term represents the uncertainty inherent in the measurement process. Then the mean difference in residence times may be written in terms of the experimentally obtained quantities:

$$\langle \Delta T \rangle = \langle \Delta T_n \rangle + \delta \langle \Delta T_n \rangle, \quad (17)$$

where  $\langle \Delta T_n \rangle = \langle T_{n+} \rangle - \langle T_{n-} \rangle$ . We can easily obtain from (16),

$$\delta \langle \Delta T_n \rangle = \sqrt{\delta T_{n+}^2 + \delta T_{n-}^2} = \sqrt{\frac{\sigma_{T_{n+}}^2 + \sigma_{T_{n-}}^2}{N}} \approx \sigma_{T_n} \sqrt{2/N}, \quad (18)$$

where we set  $\sigma_{T_{n+}} \approx \sigma_{T_{n-}} = \sigma_{T_n}$ , since the distributions are identical with the separation of means being the only manifestation of the presence of the target signal.

Now, we introduce an output signal-to-noise ratio (SNR) via the definition,

$$SNR = \frac{\langle \Delta T_n \rangle}{\delta \langle \Delta T_n \rangle} = \frac{\langle \Delta T_n \rangle}{\sigma_{T_n}} \sqrt{\frac{N}{2}}. \quad (19)$$

We assume that we are given a finite observation time  $T_{ob} = 2N \frac{T_+ + T_-}{2}$ , whence we can obtain

$$N = \frac{T_{ob}}{T_+ + T_-} = \frac{T_{ob}}{\langle \Delta T_n \rangle + 2 \langle T_- \rangle} \approx \frac{T_{ob}}{2 \langle T_- \rangle}. \quad (20)$$

Hence, we finally obtain for the SNR (note that it is a function of all the system parameters, and, specifically of the bias signal amplitude  $A$ ):

$$SNR = \frac{1}{2} \frac{\langle \Delta T_n \rangle}{\sigma_{T_n}} \sqrt{\frac{T_{ob}}{\langle T_{n-} \rangle}}. \quad (21)$$

It is of interest to compute and analyse the SNR (21) as a function of the bias amplitude  $A$  and other system parameters, as a means to optimizing performance. The simple threshold description of the ST as well as the potential-based models (mean-field and equivalent standard quartic) affords us an analytic computation of the SNR, which we now describe. It is most important to reiterate, at this point, the stringent constraints on our use of the threshold descriptions (4), (12), and (13). For all three models, the noise standard deviation must be

small compared to the threshold “height”, with  $A$  being suprathreshold. In addition, the replacement of the dynamics (1) and (9) by the simple static threshold descriptions that lead to the deterministic results (12) and (13) are predicated on a bias signal amplitude that is suprathreshold. To get an analytical estimate of the SNR (21), we resort to our simple ST model described in section 2. We assume the noise-floor to be small (compared to the threshold setting), and to manifest itself in a fluctuating threshold with mean value  $b$ ; the fluctuations are assumed to be Gaussian:

$$P(\zeta) = \frac{1}{\sqrt{2\pi}\sigma^2} \exp\left\{-\frac{(\zeta - b)^2}{2\sigma^2}\right\}. \quad (22)$$

Let us first consider the case of sinusoidal bias signal. Assuming that we start at  $t = 0$ , the first  $t_1$ , to the upper threshold (at  $+b$ ) is now a random variable; its probability may be readily computed [16] via a change of variables, wherein the mean crossing time is well-approximated by the deterministic crossing time as derived in section 2:

$$P(t_1) = \frac{\omega A}{\sqrt{2\pi}\sigma^2} \cos \omega t_1 \exp\left\{-\frac{A^2}{2\sigma^2}(\sin \omega t_1 - \sin \omega t_{10})^2\right\}, \quad (23)$$

which is normalized to unity over the interval  $0 \leq t_1 \leq T_0/4$ , which contains the first crossing to the upper threshold, since the signal is well suprathreshold; note that  $P(t_1) = 0$  outside this interval. In an analogous manner, we obtain the first crossing time probability for the lower threshold:

$$P(t_2) = \frac{\omega A}{\sqrt{2\pi}\sigma^2} \cos \omega t_2 \exp\left\{-\frac{A^2}{2\sigma^2}(\sin \omega t_2 - \sin \omega t_{20})^2\right\}, \quad (24)$$

normalized to unity in  $T_0/2 \leq t \leq 3T_0/4$ . Note that these density functions tacitly assume a deterministic threshold crossing picture of the form described in section 2. The bias signal must be well suprathreshold and the noise intensity  $\sigma^2$  also should be small compared to the threshold height. In (23) and (24), the deterministic crossing times  $t_{1,20}$  are given by (3).

In terms of the density functions (23) and (24), we may write down formal expressions for the mean crossing times  $\langle t_1 \rangle_{th}$  and  $\langle t_2 \rangle_{th}$ , the subscript denoting the theoretical (in this case, approximate) quantity:

$$\langle t_1 \rangle_{th} = \int_0^{T_0/4} P(t_1) t_1 dt_1, \quad (25)$$

and,

$$\langle t_2 \rangle_{th} = \int_{T_0/2}^{3T_0/4} P(t_2) t_2 dt_2. \quad (26)$$

The theoretical difference in residence times is then,

$$\begin{aligned} \langle \Delta T \rangle_{th} &= \langle T_+ \rangle_{th} - \langle T_- \rangle_{th} \\ &= 2(\langle t_2 \rangle_{th} - \langle t_1 \rangle_{th}) - T_0, \end{aligned} \quad (27)$$

in terms of the definitions (25) and (26). The standard deviation in the denominator of (21) is computed via the second moment of  $t_1$ :

$$\sigma_{T_n} \approx \sqrt{2(\langle t_1^2 \rangle_{th} - \langle t_1 \rangle_{th}^2)} \equiv \sqrt{2\sigma_{t_1}^2}, \quad (28)$$

and the remaining term in the denominator of the square root factor in (21) replaced by the difference in the mean crossing times.

The integrals above must be computed numerically, in general. We then readily observe that in the limit of small noise variance and large bias amplitude, the averaged quantities are well-approximated by their deterministic counterparts (defined in section 2):

$$\langle t_{1,2} \rangle_{th} \approx t_{1,20}, \quad \langle \Delta T \rangle_{th} \approx \Delta T_{ST0}, \quad (29)$$

where the deterministic residence times difference is given in (4). We may also, in the regime of validity of the correspondences (29), approximately evaluate the integrals (25) and (26) using a second order Laplace expansion [35], in which we retain terms upto  $O(\sigma^2)$  only. We then obtain,

$$\begin{aligned} \langle t_1 \rangle_{th} &\approx t_{10} + \frac{\sigma^2}{A^2} \sec \omega t_{10} G_{10}(t_{10}) + h.o.t., \\ \langle t_2 \rangle_{th} &\approx t_{20} + \frac{\sigma^2}{A^2} \sec \omega t_{20} G_{20}(t_{20}) + h.o.t. \end{aligned} \quad (30)$$

For the variance  $\sigma_{t_1}^2$  we obtain,

$$\sigma_{t_1}^2 \approx \frac{\sigma^2}{A^2} \sec \omega t_{10} \{G_2(t_{10}) - 2t_{10}G_{10}(t_{10})\}, \quad (31)$$

where we have defined,

$$\begin{aligned} G_{10}(t_{10}) &= -\frac{f_1^{(2)}}{2\phi_1^{(2)}}(t_{10}) + \frac{f_1\phi_1^{(4)}}{8[\phi_1^{(2)}]^2}(t_{10}) \\ &\quad + \frac{f_1^{(1)}\phi_1^{(3)}}{2[\phi_1^{(2)}]^2}(t_{10}) - \frac{5f_1[\phi_1^{(3)}]^2}{24[\phi_1^{(2)}]^2}(t_{10}), \end{aligned} \quad (32)$$

$$\begin{aligned} G_{20}(t_{20}) &= -\frac{f_1^{(2)}}{2\phi_2^{(2)}}(t_{20}) + \frac{f_1\phi_2^{(4)}}{8[\phi_2^{(2)}]^2}(t_{20}) \\ &\quad + \frac{f_1^{(1)}\phi_2^{(3)}}{2[\phi_2^{(2)}]^2}(t_{20}) - \frac{5f_1[\phi_2^{(3)}]^2}{24[\phi_2^{(2)}]^2}(t_{20}), \end{aligned} \quad (33)$$

$$\begin{aligned} G_2(t_{10}) &= -\frac{f_2^{(2)}}{2\phi_1^{(2)}}(t_{10}) + \frac{f_2\phi_1^{(4)}}{8[\phi_1^{(2)}]^2}(t_{10}) \\ &\quad + \frac{f_2^{(1)}\phi_1^{(3)}}{2[\phi_1^{(2)}]^2}(t_{10}) - \frac{5f_2[\phi_1^{(3)}]^2}{24[\phi_1^{(2)}]^2}(t_{10}), \end{aligned} \quad (34)$$

and,

$$\begin{aligned} f_1(t) &= t \cos \omega t, & f_2(t) &= t^2 \cos \omega t \\ \phi_1(t) &= -\frac{1}{2}(\sin \omega t - \sin \omega t_{10})^2 \\ \phi_2(t) &= -\frac{1}{2}(\sin \omega t - \sin \omega t_{20})^2. \end{aligned} \quad (35)$$

In the above expressions, the superscripts (e.g.  $\phi^{(m)}$ ) denote the  $m^{\text{th}}$  time derivative.

The mean crossing times (30) agree very well (in the limit of small  $\sigma/A$ ) with the values obtained by numerically evaluating the integrals (25) and (26). Good agreement is also obtained between the standard deviation  $\sigma_{t_1}$  and its numerically obtained counterpart. In fact, a glance at the equations (30) shows that at large signal amplitude (and/or small noise intensity), the crossing times approach their deterministic values  $t_{1,20}$ ; in turn, these behave as  $1/A$  for large  $A$ . In this regime of operation, the residence times density functions (23) and (24) collapse into gaussians having the form

$$P(t_1) \approx \frac{1}{\sqrt{2\pi\Sigma_s^2}} \exp \left\{ -\frac{1}{2\Sigma_s^2}(t_1 - t_{10})^2 \right\}, \quad (36)$$

which is normalized to unity on  $[-\infty, \infty]$  and where  $\Sigma_s^2 = \frac{\sigma^2}{A^2\omega^2}$ , a “dressed” variance that is seen to decrease rapidly with decreasing  $\sigma$  and/or increasing  $A$ ; the simulations of section 4 have already shown this behavior. A corresponding expression is obtained for  $P(t_2)$ . Note that simple differentiation of the densities (23) and (24) shows the modes approaching the mean values in the large  $A/\sigma$  limit. Of course we have already observed (equation (30)) that the average crossing times approach their deterministic counterparts in this limit.

In the gaussian limit, we can find a theoretical expression for the SNR. We start by computing the residence times density function for the up-state for which individual residence times are denoted by  $T_u = t_2 - t_1$ ,  $t_{1,2}$  being the individual crossing times. The density function of the residence times is obtained via the convolution

$$P(T_u) = \int_{-\infty}^{\infty} P_1(T_u - t_2)P_2(t_2)dt_2 \quad (37)$$

which, after some manipulations yields:

$$P(T_u) = \frac{1}{\sqrt{4\pi\Sigma_s^2}} \exp \left\{ -\frac{1}{4\Sigma_s^2}(T_u - t_{10} + t_{20})^2 \right\}, \quad (38)$$

An analogous expression may be computed for the residence times density function in the down-state. Then, using the expression (4), setting  $\sigma_{T_n}^2 = 2\Sigma_s^2$ , and taking  $\langle T_+ \rangle = t_{20} - t_{10}$  (with the deterministic crossing times defined in (3)), we obtain the theoretical SNR as

$$SNR = \frac{1}{2} \frac{A\omega}{\sigma} \frac{\Delta T_{ST0}}{\sqrt{T_0 - \Delta T_{ST0}}} \sqrt{T_{ob}}. \quad (39)$$

It is instructive to repeat the theoretical calculations using the waveform (6) as the bias signal. One may compute the residence times density function in a manner analogous to the above. Starting with the expression (22) for the noise probability density function, we may obtain the crossing times density functions via a simple change of variables:

$$P(t_{1,2}^{(i)}) = \frac{1}{\sqrt{2\pi\Sigma_i^2}} \exp \left\{ -\frac{1}{2\Sigma_i^2}(t_{1,2}^{(i)} - t_{1,20}^{(i)})^2 \right\}, \quad (40)$$

which is also normalized to unity on  $[-\infty, \infty]$ . Here, we have introduced, as we did for the sinusoidal bias case above, the “dressed” variance parameter  $\Sigma_i^2 \equiv \frac{\pi^2\sigma^2}{\omega^2\kappa_2^2}$ .

Denoting by  $T_u^{(i)} = t_2^{(i)} - t_1^{(i)}$  the residence time in the up-state, one obtains its density function in a manner analogous to that used above for (38):

$$P(T_u^{(i)}) = \frac{1}{\sqrt{4\pi\Sigma_i^2}} \exp \left\{ -\frac{1}{4\Sigma_i^2}(T_u^{(i)} - t_{10}^{(i)} + t_{20}^{(i)})^2 \right\}, \quad (41)$$

which is gaussian having mean  $t_{20}^{(i)} - t_{10}^{(i)}$  and variance  $2\Sigma_i^2 = \frac{2\pi^2\sigma^2}{\omega^2\kappa_2^2}$ . We readily observe that  $\langle \Delta T^{(i)} \rangle \rightarrow 0$  and  $t_{20}^{(i)} - t_{10}^{(i)} \rightarrow T_0/2$  when  $\varepsilon \rightarrow 0$ , as expected. The separation between the peaks in the residence times density function is given by (8) exactly as predicted for the noise-free case. The SNR (21) may now readily be estimated for this waveform. We find,

$$SNR = \frac{1}{2} \frac{\kappa_2\omega}{\pi\sigma} \frac{\Delta T^{(i)}}{\sqrt{T_0 - \Delta T^{(i)}}} \sqrt{T_{ob}}. \quad (42)$$

The similar structure of equations (39) and (42) should be noted. Note, also, that the SNR behaves like  $A/\sigma$  for the sinusoidal waveform, and like  $\kappa_2/\sigma$  for the alternate waveform (6). Hence, one obtains a performance enhancement with decreasing noise intensity for both signal waveforms, as might be expected. For the sinusoidal bias signal, one can increase the SNR further, by increasing the bias amplitude  $A$ , however this must be weighed against the requirement of lower power consumption as well as the resolvability of  $\langle \Delta T \rangle$ : with increasing  $A$ ,  $\langle \Delta T \rangle$  decreases and the lobes of the RTD converge to a single sharp peak at  $T_0/2$ . For the waveform (6) the situation is more complex, as seen in figure (5); given a noise-floor, the response might be expected to increase with increasing  $\kappa_2$ , peaking at the critical value of  $\kappa_{2c} \approx \frac{1}{2}(A - b - \varepsilon)$ , and then decreasing. The SNR in both cases is proportional to  $\sqrt{T_{ob}}$ ; increasing  $T_{ob}$  leads to improved statistics, although operational constraints in specific applications may limit its magnitude.

It is of interest to actually find some measure of comparison between the readout schemes that employ the RTDs as described in this work, and more conventional readout schemes (see section 1) based on the output

power spectral density (PSD). Such a comparison is possible in the context of a rigorous statistical analysis of the device response; we address this in the next section.

## VI. RESIDENCE TIMES ASYMMETRY OR POWER SPECTRAL DENSITY? A PERFORMANCE COMPARISON FOR DIFFERENT READOUT SCHEMES

As shown in the previous sections, the bias signal waveform (6) can improve the performance (based on the separation  $< \Delta T >$  of the mean residence times) of this readout scheme under the appropriate conditions. We now investigate whether this is sufficient to make the RTD-based technique competitive with conventional readout schemes based on the PSD. In order to carry out this comparison we must abandon the (somewhat simplistic) ST and, instead, analyse one of the potential systems (2) or (10), together with a more general performance measure. Since both potential systems behave similarly we have used the equivalent Duffing potential (10) which is somewhat easier to analyse. We start with a stochastic perturbation expansion of the dynamical system; this leads us to expressions for the probability density functions of the crossing times between the stable states. The residence times based readout scheme will be seen to be, at least asymptotically, as good as any other readout scheme based on time measurements. Finally the residence time based scheme and the ‘‘conventional’’, i.e. based on the PSD, scheme are compared via Monte Carlo simulations.

### A. Stochastic Perturbation Expansion

We start by introducing a stochastic process  $Z = (\zeta_t, \eta_t, x_t)$  in  $R^3$ . The system described by equations (9), (10), and (14) can then be written in the form of an (Itô) stochastic differential equation (SDE)

$$dZ_t = g_1(Z_t) dt + \sigma g_2(Z_t) dW_t, \quad Z_0 = z_0, \quad (43)$$

where  $Z$  componentwise is defined by

$$\begin{pmatrix} d\zeta_t \\ d\eta_t \\ dx_t \end{pmatrix} = \begin{pmatrix} -\tau_c^{-1} \zeta_t \\ 1 \\ ax_t - bx_t^3 + \varepsilon + h_t + \gamma \zeta_t \end{pmatrix} dt + \sigma \begin{pmatrix} 1 \\ 0 \\ 0 \end{pmatrix} dW_t. \quad (44)$$

Here  $\sigma$  is assumed to be a small noise standard deviation and the second equation only expresses time as a state variable. The asymptotic properties for  $\sigma \rightarrow 0$  of equations such as (43) have been analyzed in [36]. If  $\xi$  now is used as the formal time derivative of the Brownian motion  $W$ , equation (43) can be written as

$$\dot{Z}_t = g_3(Z_t, \sigma \xi_t), \quad Z_0 = z_0, \quad (45)$$

where

$$g_3(u, \sigma v) = g_1(u) + \sigma g_2(u)v, \quad u \in R^3, v \in R.$$

In order to arrive at a sequence of approximations to the solution  $Z$  to (43) the following perturbation ansatz is made. The solution  $Z$  to (45) is formally expanded in terms powers of  $\sigma$  as

$$Z_t = Z_t^{(0)} + \sigma Z_t^{(1)} + \dots + \sigma^k Z_t^{(k)} + \dots \quad (46)$$

and the right hand side of (45) is, accordingly, also expanded in terms of powers of  $\sigma$ . If the coefficients on both sides of the arisen equality

$$\begin{aligned} \dot{Z}_t^{(0)} + \sigma \dot{Z}_t^{(1)} + \dots &= \\ &= g_3(Z_t^{(0)}, 0) + \sigma \left( \left. \frac{dg_3(Z_t^{(0)} + \sigma Z_t^{(1)} + \dots, \sigma \xi_t)}{d\sigma} \right|_{\sigma=0} \right) + \dots \\ &= g_3(Z_t^{(0)}, 0) + \sigma \left( G_{31}(Z_t^{(0)}, 0) Z_t^{(1)} + G_{32}(Z_t^{(0)}, 0) \xi_t \right) + \dots, \end{aligned}$$

are then equated the following differential equations for the correction terms (functions) emerge

$$\begin{aligned} \dot{Z}_t^{(0)} &= g_3(Z_t^{(0)}, 0), \\ \dot{Z}_t^{(1)} &= G_{31}(Z_t^{(0)}, 0) Z_t^{(1)} + G_{32}(Z_t^{(0)}, 0) \xi_t, \\ \dots &\dots, \end{aligned} \quad (47)$$

where the matrix  $G_{31}$  and vector  $G_{32}$  are given by

$$G_{31}(Z_t^{(0)}, 0) = \begin{pmatrix} -\tau_c^{-1} & 0 & 0 \\ 0 & 0 & 0 \\ \gamma & h'(t) & a - 3b(Z_t^{(0)})^2 \end{pmatrix},$$

$$G_{32}(Z_t^{(0)}, 0) = \begin{pmatrix} 1 \\ 0 \\ 0 \end{pmatrix},$$

and the initial conditions are  $Z_0^{(0)} = z_0, Z_0^{(1)} = 0, \dots$ . The details for the higher order corrections (for  $k \geq 2$ ) are easily calculated, see [36]. It turns out that all higher corrections are linear in  $\xi$  and it follows therefore that the vector process  $Z^{k+1} = (Z^{(0)}, \dots, Z^{(k)})^T$  obtained by considering simultaneously the  $k+1$  first corrections in (47) represents, formally, an SDE. In [36, Thm. 2.2] it is shown that if the components of  $g_1, g_2$  have bounded partial derivatives up to  $k+1$ :th order (inclusive), then the SDE for  $Z^{k+1}$  is in fact well-defined with a strong solution and the component  $\sum_{i=0}^k \sigma^i Z^{(i)}$  is an approximation to  $Z$  for which the error is asymptotically small in mean square as  $\sigma \rightarrow 0$ . Therefore a  $k$ :th order expansion like (46) will henceforth be denoted as

$$Z_t = Z_t^{(0)} + \sigma Z_t^{(1)} + \dots + \sigma^k Z_t^{(k)} + O(\sigma) \quad (48)$$

where the remainder term is primarily to be interpreted as asymptotically small in a mean squared sense.

## B. First Order Approximation

From (47) it is seen that the zero order approximation is simply the deterministic ordinary differential equation (ODE) that would be obtained by setting  $\sigma = 0$  in (43), and that the first order approximation is obtained by linearizing (43) around the nominal deterministic trajectory obtained from the order zero approximation. We now study the first order approximation and suppose that (48) holds for  $k = 1$  and that  $z_0$  is an interior point of a domain  $D$  in  $R^3$  such that the first exit time  $t_0$  of the process  $Z_t^{(0)}$  from  $D$  is finite. Suppose further that the boundary is differentiable at  $Z_{t_0}^{(0)}$ , let  $\bar{n}$  be the exterior normal to the boundary at  $Z_{t_0}^{(0)}$  and denote the first exit time of the process  $Z_t$  from  $D$  by  $\tau_\sigma$ . Then if  $(\dot{Z}_{t_0}^{(0)}, \bar{n}) > 0$  we have [36],

$$\tau_\sigma = t_0 + \sigma \frac{(Z_{t_0}^{(1)}, \bar{n})}{(\dot{Z}_{t_0}^{(0)}, \bar{n})} + O(\sigma), \quad (49)$$

where the remainder term should be interpreted in the sense used in (48). Hence the first passage time problem for the time varying potential with colored noise can be formulated as the problem of determining  $\tau_\sigma$  in (49) when  $x_0 < x_{limit}$ , where  $x_{limit}$  is a barrier for the variable  $x$ . In this case  $\bar{n}$  becomes simply  $\bar{n} = (0, 0, 1)^T$  and the condition  $(\dot{Z}_{t_0}^{(0)}, \bar{n}) > 0$  in (49) reduces to  $\dot{x}_{t_0}^{(0)} > 0$  where  $x^{(0)}$  is the last component in the solution to the first equation in (47).

Since  $W$  is a gaussian process, so is the first order approximation  $x^{(1)}$ , and the first passage time  $\tau_\sigma$  is therefore a gaussian variable with mean  $t_0$  and a variance

$$V(\tau_\sigma) = \sigma^2 \frac{E(x_{t_0}^{(1)})^2}{(\dot{x}_{t_0}^{(0)})^2}. \quad (50)$$

Further, the (unique) solution to the second equation in (47) is well-known to be (see e.g. [36]),

$$Z_t^{(1)} = \int_0^t \Phi(t, r) g_2(Z_r^{(0)}) dW_r, \quad (51)$$

where  $\Phi(t, s)$  is the transition matrix from time  $s$  to  $t$  for the flow (smooth vector field) on  $R^3$  defined by

$$\dot{Z}_t^{(1)} = G_{31}(Z_t^{(0)}, 0) Z_t^{(1)}.$$

In this case the transfer matrix  $\Phi$  is given by

$$\Phi(s, t) = \exp\left(-\int_s^t G_{31}(Z_r^{(0)}, 0) dr\right).$$

Hence (51) can be written as

$$Z_t^{(1)} = \int_0^t \exp\left(-\int_q^t G_{31}(Z_r^{(0)}, 0) dr\right) g_2(Z_q^{(0)}) dW_q,$$

and (50) therefore becomes

$$\begin{aligned} V(\tau_\sigma) &= \sigma^2 \frac{\int_0^{t_0} \bar{n}^T \Phi(t_0, r) g_2(Z_r^{(0)}) g_2^T(Z_r^{(0)}) \Phi^T(t_0, r) \bar{n} dr}{(\dot{x}_{t_0}^{(0)})^2} \\ &= \sigma^2 \frac{\int_0^{t_0} (\Phi_{3,1}(t_0, r))^2 dr}{(\dot{x}_{t_0}^{(0)})^2}, \end{aligned} \quad (52)$$

where  $\Phi_{3,1}(t_0, r)$  is the third row, first column element of  $\Phi(t_0, r)$ . This element is plotted against the normalized time  $t/T_0$  in fig. 6.

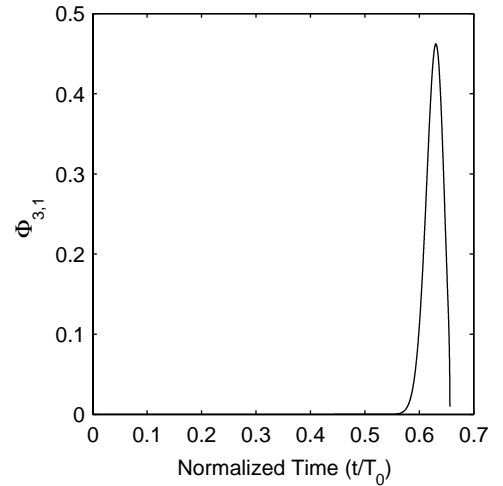


FIG. 6. The element  $\Phi_{3,1}(t_0, t)$  versus  $t/T_0$  for  $\varepsilon = 0$ ,  $\sigma^2 = 0.01$ ,  $A = 0.8$ ,  $\gamma = 1$ ,  $T_0 = 100$ , start time = 0, and the parameters  $a, b$  for the equivalent Duffing potential are computed via (11), for  $c = 4$  in the mean field potential (2).

Since we have assumed a clearly suprathreshold bias signal the previous crossing time, i.e. the start time, will be in  $[0, T/2]$ . For all such starting times numerical calculations show that the next deterministic crossing time  $t_0$  is reasonably independent of the starting time [18]. Further, as seen in figure 6, the function  $\Phi_{3,1}$  is close to zero for all  $t \in [0, T/2]$  and therefore the integral in (52) will also be almost independent of the starting time. Hence all crossing times will be approximately independent and gaussian distributed with means and variance given by (49) and (52), respectively. This has, of course, already been observed in our crude (Schmidt trigger) model of the preceding section in the large  $A/\sigma$  limit, when  $A$  is well-suprathreshold.

## C. Analysis of Time Based Readout

The approximate crossing times distributions calculated in the previous section are important when evaluating performance measures for “time-based” devices. Since we also want to compare the performance of these devices with the one obtained under different readout

schemes, we have to abandon the SNR in (21) and move on to a more general performance measure. There exist several possible ways to define such a measure, however, since the expected value of the estimations is correct it seems natural to apply the classic MMSE [38] (Minimum-Mean-Squared-Error Estimation) formalism, and consider the estimator with the lowest variance of the result to be the best. Note, though, that the variance associated with all the estimators, will decrease towards zero when the observation time increases. Therefore a finite observation time  $T_{ob}$  is used, and the goodness criteria of the sensors is defined as the variance of the estimation given this observation time.

For residence times based devices there will be  $n(T_{comp})$  switches between the stable states during the observation time. As previously shown, all crossing times will be approximately gaussian distributed with a mean that depends on the target signal and a variance as in (52). The dependence between the separation of the mean crossing times and the target signal is linear for small asymmetrizing target signals, i.e.,

$$\varepsilon = \mu c_l, \quad (53)$$

where  $\mu$  is the change of crossing time and  $c_l$  a constant. This has already been mentioned in an earlier section, and it can be confirmed by a numerical simulation of the system. The crossing times independence therefore affords the possibility of extracting the optimal achievable limit for any kind of estimator based on crossing times. Let us define  $\bar{u}_i$  and  $\bar{d}_i$  as  $\bar{u}_i = u_i - u_0 \bmod(T_0)$  and  $\bar{d}_i = d_i - d_0 \bmod(T_0)$ ,  $i \geq 1$ , where  $u_i$  and  $d_i$  are the two (different) crossing times, from one state to the other, and from the second back to the first. Here  $u_0$  and  $d_0$  are the first crossing times in the noise-free system in the absence of the dc target signal. It is readily obtained that  $\mu_{cross} = \mu_u = -\mu_d$  (where  $\mu_u = E(\bar{u}_i)$  and  $\mu_d = E(\bar{d}_i)$ ) and  $\sigma_{cross} = \sigma_u = \sigma_d$  (where  $\sigma_u^2 = V(\bar{u}_i)$  and  $\sigma_d^2 = V(\bar{d}_i)$ ). The set  $\{\bar{u}_1, \bar{u}_2, \dots, \bar{u}_{n+1}, -\bar{d}_1, -\bar{d}_2, \dots, -\bar{d}_n\}$  will then consist of  $2n + 1$  independent identically distributed Gaussian variables with mean  $\mu_{cross}$  and variance  $\sigma_{cross}^2$ . In this case it is known from (53) that the minimum variance estimator of  $\varepsilon$  is given by

$$\bar{\varepsilon}_{opt} = \frac{\sum_{i=1}^{n+1} \bar{u}_i - \sum_{i=1}^n \bar{d}_i}{2n + 1} c_l,$$

with a variance

$$V(\bar{\varepsilon}_{opt}) = \frac{c_l^2 \sigma_{cross}^2}{2n + 1}, \quad (54)$$

which is easily proved by e.g. the information equality [37].

In the previously described approach which measures the mean difference in residence times  $\langle \Delta T \rangle$ , a displacement  $\mu_{cross}$  for the crossing times results in a mean residence time difference of  $4\mu_{cross}$ . The estimate of the

target signal therefore becomes  $\bar{\varepsilon}_{res} = \frac{c_l}{4} \Delta T$ , where

$$\Delta T = \frac{1}{n} \left( \sum_{i=1}^n (d_i - u_i) - \sum_{i=1}^n (u_{i+1} - d_i) \right).$$

The variance of the residence times based estimator will then be

$$V(\bar{\varepsilon}_{res}) = V(c_l \frac{\Delta T}{4}) = \frac{c_l^2}{16} V(\Delta T)$$

where  $V(\Delta T) = V(\frac{1}{n} \sum_{i=1}^n (2d_i - u_i - u_{i+1}))$ , which, with the definition  $Y_i = 2d_i - u_i - u_{i+1}$ , becomes

$$\begin{aligned} V(\Delta T) &= V\left(\frac{1}{n} \sum_{i=1}^n (Y_i)\right) \\ &= \frac{1}{n^2} \left( \sum_{i=1}^n V(Y_i) + \sum_{i \neq j} \sum_{j=1}^n Cov(Y_i, Y_j) \right), \end{aligned}$$

which by straight forward calculations can be shown to be

$$V(\Delta T) = \frac{8\sigma_{cross}^2}{n} - \frac{2\sigma_{cross}^2}{n^2}.$$

Hence, the residence times based estimator has the variance

$$V(\bar{\varepsilon}_{res}) = \frac{c_l^2}{16} \left( \frac{8\sigma_{cross}^2}{n} - \frac{2\sigma_{cross}^2}{n^2} \right) = \frac{c_l^2 \sigma_{cross}^2}{2n} - \frac{c_l^2 \sigma_{cross}^2}{8n^2},$$

which is slightly worse than the optimal time based estimator, (54), although the performance is comparable (asymptotically) for large  $n$  and is much easier to implement in an experiment. In most cases the residence time based readout can, therefore, be considered to be the optimal time based readout.

#### D. Comparison of Different Readouts

In the previous section we illustrated the advantage of applying the residence times based readout scheme, if only sensors involving time measurements were considered. However, it is also instructive to analyse how this readout performs compared to other, more conventional, readout schemes, and to determine the optimal amplitude of the bias signal. Such an investigation is likely to be quite exhaustive, and beyond the scope of the current paper. However, a good starting point is to compare the residence times based readout scheme with a ‘‘conventional’’ (PSD-based) readout, when a time-sinusoidal bias signal is applied in each case. This computation will just show the most appropriate amplitude of the sinusoidal bias, with the frequency kept fixed for both devices. This investigation can later easily be expanded to encompass larger signal families.

To compare the readouts,  $n_{sim}$ , output trajectories  $x_t, t \in [0, T_{ob}]$  are calculated for each amplitude of the

driving signal. Based on these trajectories  $n_{sim}$ , estimates of the target signal  $\varepsilon$  are calculated with both the residence times technique and the conventional (PSD-based) technique, for each amplitude. The variances of these estimates which, according to the preceding subsection, could be used as performance measures, are then used to establish the best bias signal amplitude for each method. However, it is also of interest to know how close the sensors are to the *optimal* performance limit. The optimal performance is given by the MMSE estimator of  $\varepsilon$  based on observations of  $x_t$  over  $[0, T_{ob}]$ . In case the target signal  $\varepsilon$  is a zero mean Gaussian random variable, independent of both the initial condition  $x_0$  and the driving noise, the optimal performance is easy to calculate if the noise is white. Therefore, if we instead of adding the colored noise process  $\zeta_t$  to the state increment  $dx_t$  in (44) add a (scaled) Brownian motion increment  $\sigma_{wg}dW_t$  we obtain the following (“white noise”) model on SDE form

$$dx_t = (f(x_t) + \varepsilon + h_t)dt + \sigma_{wg}dW_t,$$

where the function  $f$  represents the Duffing potential,  $f(x) = ax - bx^3$ . The MMSE  $\hat{\varepsilon}$  of  $\varepsilon$  based on  $x_t, t \in [0, T_{ob}]$  for a system of this type is well-known [39, sec. 17.7] and given by

$$\hat{\varepsilon} = \frac{x_{T_{ob}} - x_0 - \int_0^{T_{ob}} (f(x_t) + h_t) dt}{\frac{\sigma_{wg}^2}{\sigma_\varepsilon^2} + T_{ob}}, \quad (55)$$

where  $\sigma_\varepsilon^2$  is the variance of the zero mean Gaussian random variable  $\varepsilon$ . When  $\sigma_\varepsilon^2 \rightarrow \infty$  the formula (55) becomes identical with that for the Maximum Likelihood (ML) estimate of  $\varepsilon$  [39, sec. 17.7]. Thus, the ML estimator, which is well-defined also when  $\varepsilon$  is considered as an unknown constant, is a limiting case of the optimal MMSE estimator in (55) which is obtained when  $\sigma_\varepsilon^2 \rightarrow \infty$  (i.e. when  $\varepsilon$  becomes “completely unknown”). The variance of the ML estimator therefore provides a lower bound on the achievable performance of any estimator of  $\varepsilon$  when  $\varepsilon$  is an unknown constant.

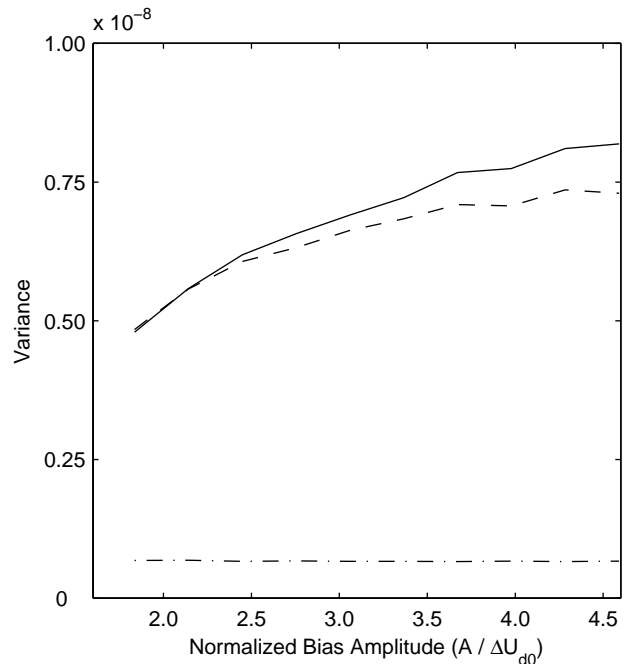


FIG. 7. The variance of the estimations versus the sinusoidal bias signal amplitude for the residence times based (solid line), PSD based (dashed line), and MLE based (bottom dash-dotted line) method. Here the parameters  $a, b$ , and  $\omega$  are as in figure 6,  $\gamma = 1$ ,  $T_{ob} = 3000$ , and the white noise intensity is  $\sigma_{wg} = \sqrt{2} \cdot 10^{-6}$ .

In fig. 7 the variance of the estimates versus driving signal amplitude is shown for the two different kinds of readout schemes (residence times, and PSD-based) and the MLE. As seen, the residence times based readout is nearly as good as the PSD-based case, although the sinusoidal bias signal may not be optimal for this sensor (at least under the parameters considered here). A triangular wave, or the waveform (6) should improve the results; as already discussed, these waveforms provide local linearity where the waveform crosses the threshold. Clearly though, both devices perform much worse than the MLE, and it is obvious that both measuring techniques are non-optimal. From these data it therefore would appear that a MLE-based readout, or a residence times based readout with a carefully selected driving signal, would be preferable compared to a PSD-based readout. However, one very surprising result indicates that care should be taken when interpreting the data. The variance of the estimates *decreases* when the bias amplitude decreases, implying that a weak bias amplitude might be preferable. For the PSD-based readout this is a counterintuitive result since in practical scenarios these sensors are normally driven with a large amplitude bias signal. It is therefore possible that the simple models of section 2 that we use to describe our sensors, may not be good enough. In this context it should be noted that in real sensors involving, e.g., ferromagnetic cores, the noise-floor is usually dependent on the driving signal. This is also indicated by the

experimental results shown in figure 10. In addition, the driving signal, if applied at a sufficiently high frequency, can lead to frequency-dependent hysteresis behavior in the device, behavior that has not been covered by our phenomenological description. Clearly, an investigation of these issues should precede a rigorous investigation (beyond the relatively simple discussions, in this paper, of the system response to non-sinusoidal waveforms, exemplified by the signal (6)) into the optimal signal waveform for a particular readout scheme. However, despite these unresolved issues, we can at least conclude that the time series of the output voltage from the fluxgate probe seems to contain more information about the target signal than what can be extracted via conventional (PSD-based) and residence times based readouts.

## VII. EXPERIMENTS

In order to reconcile some of the ideas of this paper to experimental data some preliminary experiments were performed on a test device, a very simple laboratory realization of a residence times based fluxgate magnetometer. A pre-magnetizing coil with 50 turns and a pick-up coil with 135 turns were wound in a transformer-like configuration on a multi-domain ferromagnetic strip-wound ring core characterized by a coercivity of less than 3 A/m. The diameter and the cross-sectional area of the ring were 26 mm and  $1.9 \times 2.8 \text{ mm}^2$ , respectively. A ring core probe used in this configuration is not expected to possess full directional sensitivity and response to external fields [2]. It can, however, serve the purpose of demonstrating the basic principle, without making any claims on living up to the possible operational performance of a fluxgate magnetometer of this type. Note that new, improved probes based on straight rod cores are under fabrication, and the results for these devices will be published later.

A function generator producing a triangular wave with variable amplitude  $A$  and frequency was connected to the input of the device. A frequency of 100 Hz was used for all measurements; this allows one to use a non-frequency based description of the crossing dynamics, since frequency-dependent hysteresis in the core response is very small and also the bias signal has a minimal effect on the noise floor. The noise floor is assumed to be gaussian bandlimited, which is a good assumption for the new genre of “single-domain” ferromagnetic probes; non-gaussian (i.e. Barkhausen) noise may in fact be present in these cores, but it is significantly smaller (in rms amplitude) than the gaussian noise. The 100Hz driving frequency also ensures that the bias signal does not fall into the low-frequency noise riser.

The time evolution of the input current and the output voltage were measured with a 16-bit A/D-converter using a sampling rate of 40 kHz. Alternatively, the pick-up coil was connected to a universal counter for measuring the

residence times  $T_+$  and  $T_-$ . The bias field was estimated from the input current by applying Ampere’s law on the ring geometry.

The zero target measurements were performed inside a shielded cage consisting of concentric shells made of  $\mu$ -metal and copper. The measurements with target signal were performed in the presence of the geomagnetic field, which served as the target. They were made after maximizing the effective target strength by simply rotating the device until a maximum difference between  $\langle T_+ \rangle$  and  $\langle T_- \rangle$  was found; at the location of the experiment this corresponded to a field strength of about 50  $\mu\text{T}$  (the magnitude of the geomagnetic field).

Figure 8 shows the output voltage from the pick-up coil for four different amplitudes – two subthreshold and two suprathreshold – of the bias signal resulting in non-saturated and saturated magnetization, respectively. These measurements were performed without target field. The output voltage (this is our experimental observable), which is proportional to the derivative of the magnetic flux in the core, consists a number of successive spikes corresponding to switches between positive and negative magnetization (relative to the magnetic state when the bias signal was applied). A shift of the spike positions from the extrema towards the zero-crossings of the bias signal can be observed as the core material is gradually driven deeper into saturation. For the highest bias amplitude the saturated flux density is rapidly reached and the (sharp) spikes nearly coincide with the zero-crossings of the bias signal.

The time evolution of the magnetic flux density  $B$  in the core material and the magnetization curves were calculated from the experimental data by integrating the output voltage from the pick-up coil. For each set of data the unknown integration constant was assigned a value in order to make the times series of  $B$  centered around zero. The results for two amplitudes of the bias signal ( $A = 2$  and 20 A/m, corresponding to nearly saturated and saturated cores, respectively) are shown as solid curves in figure 9. Due to hysteresis effects (irreversible magnetization) changes in the magnetic flux  $B$  in the core “lag behind” changes in the magnetizing bias field  $H$ . In figure 9 this can be observed as a distortion of  $B$  from the triangular form of the bias signal and the appearance of hysteresis loops in the magnetization curves. For the saturated case (right panels)  $B$  has nearly a rectangular wave form and long tails develop in the magnetization curves.

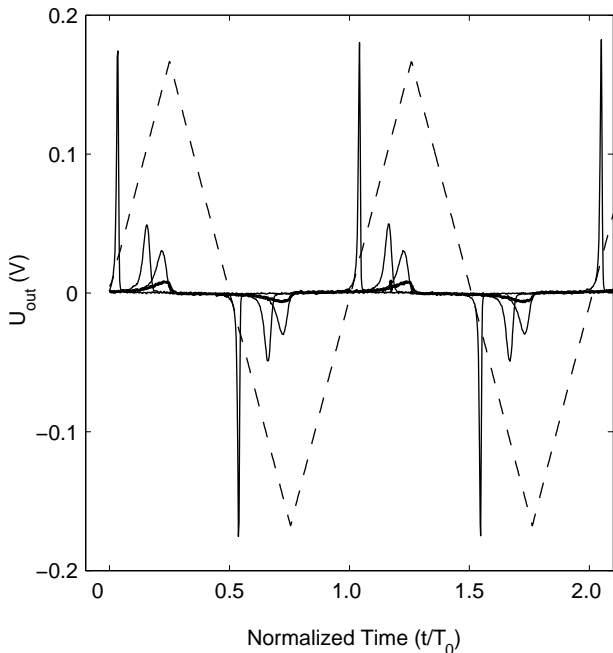


FIG. 8. Output voltage from the pick-up coil for four different amplitudes of the bias field. From left to right  $A \approx 20, 3.3, 2.0,$  and  $1.4$  A/m. Bias period  $T_0 = 0.01$  s. The dashed curve is a guide for the eyes, and indicates the phase of the bias field.

In order to study the ability of the mean field model with the "soft" potential (equation 2) to reproduce the experimental details of the ferromagnetic behavior of the core, simulations of  $B$  versus time and hysteresis loops were made. In these calculations a dimensionless temperature  $T = 1/1.4$  ( $c = 1.4$ ) was used. The results are shown as dashed curves in figure 9. For the saturated case (right panels) the experimental data are quite well described by this model. For the non-saturated case (left panels), however, only the time evolution of  $B$  seems to be fairly well matched. For even lower bias amplitudes the model is unable to reproduce either the time series or the hysteresis loops. Also the equivalent quartic model is unable to reproduce the salient features of the time series and the hysteresis loops at very low (subthreshold) bias amplitudes; this model also fails at extremely high (very suprathreshold) bias amplitudes. Note, however, that despite these discrepancies, both models can reproduce, to a very good approximation, the qualitative behavior in e.g.  $\langle \Delta T \rangle$  also for very high suprathreshold bias signals.

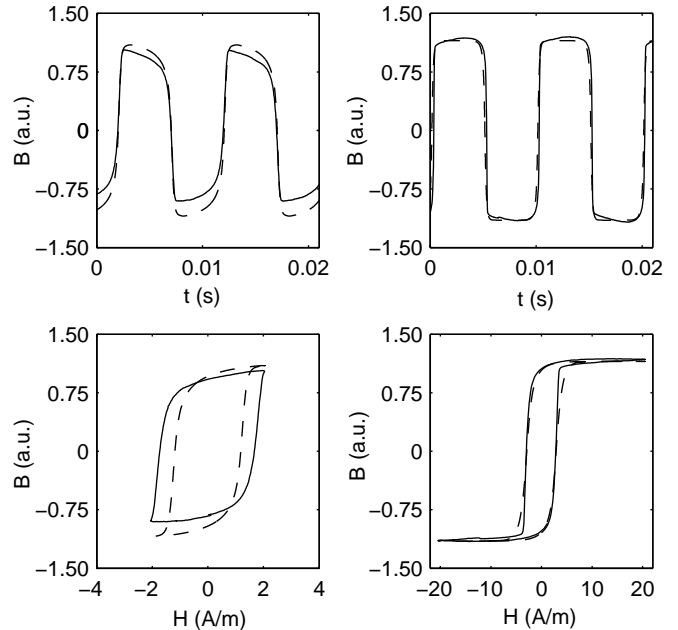


FIG. 9. Upper panels: Magnetic flux density versus time of the ferromagnetic ring core for  $A = 2$  (left panel) and  $20$  A/m (right panel). Lower panels: The same measurement results shown as hysteresis loops. Solid curves are calculated results from experimental data and dashed curves are simulated data using the "soft" potential (2) with  $c = 1.4$  and  $A = 4.0$ . Note that the B-axis has been rescaled for the simulations in order to be able to compare it to the experimental data.

Figure 10 shows the (gaussian-like) residence time distributions for three different bias amplitudes  $A$ . The data were compensated for off-sets (in the range of about  $0.5$  to  $30 \mu\text{s}$ , with the larger value corresponding to the case of the weakest bias signal) which were obtained from zero-field measurements inside the shielded cage. In all cases, the center RTD corresponds to the case of zero target signal. In the presence of a target signal the residence times  $T_+$  and  $T_-$  are different, and consequently the quantity  $\langle \Delta T \rangle = \langle T_+ \rangle - \langle T_- \rangle$  can be used as a measure of the asymmetry-producing target field. Within our experimental precision a linear relationship between the target signal and  $\langle \Delta T \rangle$  was found. This is in good agreement with expectations for a pulse position based read-out technique [2]. Such a relationship should be expected (as already discussed) from the RTD-based readout when  $\epsilon$  is small; it has already been theoretically computed in the limiting case of zero bias signal [9]. From the slope of a linear fit to the data a response of about  $7 \text{ ns}/\mu\text{T}$  for our simple test device was found, when it was driven with a  $10 \text{ kHz}$  bias frequency. Note that this result is not expected to be representative for a well designed device (currently under construction).

In figure 10 it can readily be seen that the effect of lowering the bias amplitude is twofold. First of all there is

an increase in  $\langle \Delta T \rangle$  for a given target signal strength, and second it leads to a wider spread in the residence times. For example, lowering the bias amplitude from 41 to 20 A/m appears to result in a performance improvement which can be observed as a larger increase in  $\langle \Delta T \rangle$  as compared to the dispersion of the RTDs, i.e. the gained response to external target fields seems to be larger than the cost due to a wider spread in the residence times. However, further lowering the bias amplitude down to 4.1 A/m (where the core material is only weakly saturated) a much larger spread in the residence times is observed, and the background noise makes its presence clearly known in the density function for small  $A$ .

There may be many reasons for this large dispersion at low bias amplitudes. One possible explanation could be that due to the less saturated core material (and possible memory effects caused by "non-complete" magnetic domain alignment along the bias field) the magnetic hysteresis loop is not well defined. This could, then, lead to varying residence times because different paths around the hysteresis loop may be taken for each cycle. Even in this situation, however, one observes a well-defined  $\langle \Delta T \rangle$  which, in an experiment, may readily be computed using the arithmetic mean of a large number  $N$  of observed crossing events. We reiterate that, in practical scenarios, a computation of the average residence times via the arithmetic mean is sufficient; it is not necessary to compute a density function and then compute the means via integration. Hence, the accuracy of the measurement of  $\langle \Delta T \rangle$  depends on the magnitude of  $N$ . Of course, the magnitude of  $N$  is constrained by the observation time as already discussed in section 5.

Despite the crudeness of the setup the experimental findings do qualitatively agree with the results of the simulations shown in figure 4. This, in turn, has led to the (currently ongoing) construction of a fluxgate magnetometer utilizing the residence-times-based read-out scheme. One important task when optimizing the bias signal for a real device would then be to find the optimum balance between the gain in responsivity and the increase in the noise level of the residence times.

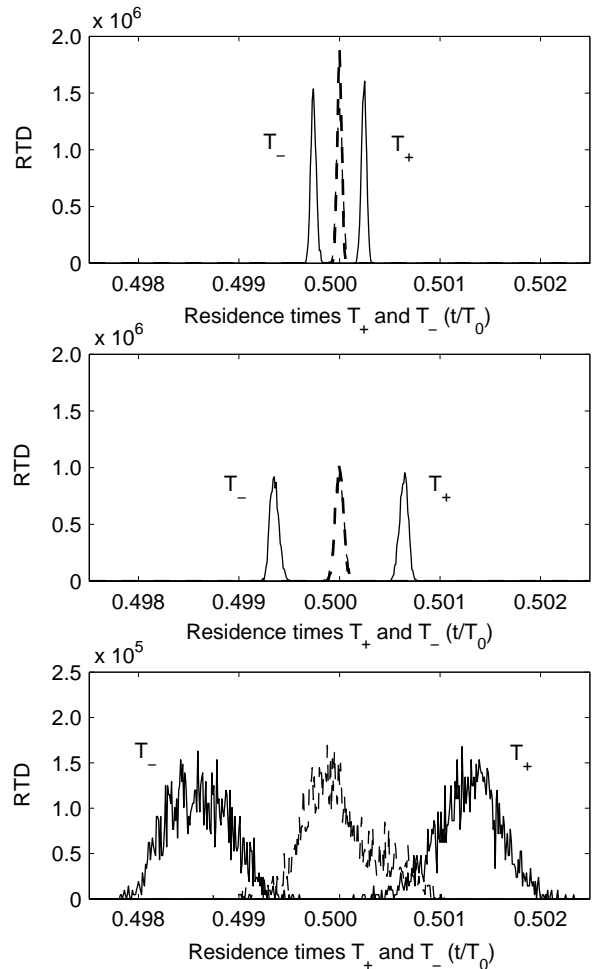


FIG. 10. Residence time distributions for three different amplitudes ( $=41, 20,$  and  $4.1$  A/m, from top to bottom panels) of the triangular bias signal. The data have been normalized to the period  $T_0 = 10$  ms. Dashed curves: Zero target case. Solid curves: Effective target field of about  $50 \mu\text{T}$ . The data have been compensated for off-sets. The effect of decreasing the bias amplitude is twofold: For a fixed target field the separation  $\langle \Delta T \rangle$  grows with decreasing bias amplitudes, at which point the fluctuations due to the noise-background also manifest themselves in the density function.

## VIII. CONCLUSIONS

In this work we have presented an alternative to quantifying the output of a nonlinear dynamic system via the power spectral density. The residence times based technique is relatively simple to implement in practical scenarios; all that is required is for the detection/processing electronics to keep track of threshold crossing events and maintain a running average, the arithmetic mean, of the residence times in each stable state. Then the quantity  $\langle \Delta T \rangle$  provides a measure of the unknown target signal that created the asymmetry and, therefore, a nonzero

$\langle \Delta T \rangle$ . While the target signal in this work is taken to be dc, it is clear that a modification of the residence-times based readout scheme could be effected for more complex signals. It is also clear that the choice of the bias signal waveform is important to the issue of overall sensitivity defined, roughly, as the ability to discriminate the means of the residence times densities in the presence of a small asymmetrizing target signal. The bias signal amplitude does not need to be extremely large. In fact our results, and those of our earlier publication [9], indicate that the best response to the target signal is obtained for zero bias signal, in theory, at least; in this scenario the level crossing events are solely controlled by the background noise. In practice, however, unless the noise level is high enough to induce an acceptable (spontaneous) crossing rate, one must impose the bias signal to control the crossings; in this case the noise leads to a spread in the crossing rate about its deterministic value, when the bias signal is suprathreshold. Clearly, in such a situation, it would be preferable to adjust the system parameters (e.g. the constant  $c$  in the potential energy function (2)) so that the energy barrier is lowered when weak target signals are to be detected in a noise-floor. Absent such a control, however, adjusting the bias amplitude  $A$ , or the triangular signal amplitude  $\kappa_2$  when we use the bias waveform 6, effectively raises or lowers the energy barrier. With a large background noise floor, the density functions tend to merge, leading to inaccuracies in the computed  $\langle \Delta T \rangle$  unless a large number  $N$  of observations can be made. Increasing  $A$  enables one to better resolve the density functions, even as it leads to a greater power requirement. Hence, one must also consider the tradeoff between sensitivity and power when designing a sensor aimed at a particular class of target signals. Noise effects become more important as the bias signal amplitude approaches the threshold; the RTD is no longer gaussian, it develops tails and its mean and mode separate.

A theoretical computation of  $\langle \Delta T \rangle$  has been carried out in the regime of large (suprathreshold) bias signal and small noise; in this (gaussian) limit, the dynamical system is well-approximated by a non-dynamical dual-threshold representation. For small target signals one easily obtains  $\langle \Delta T \rangle \propto \epsilon$ . The separation  $\langle \Delta T \rangle$  is, further, very weakly dependent on the noise in the large  $A/\sigma$  limit (the gaussian limit that has featured so prominently in our discussion). In this limit, the noise *statistics*, also, do not have a significant effect on  $\langle \Delta T \rangle$ . For subthreshold bias signals, the theory of this paper breaks down. In practical operation however, one can still compute  $\langle \Delta T \rangle$  by simple averaging as done for the suprathreshold bias case; in this case, however, the mean value separation is noise-dependent and one may optimize it using the SR scenario [6]. The RTD for subthreshold bias signals can be multimodal (depending on the noise variance, signal amplitude and potential barrier height), however, in the optimal case it collapses into a single near-gaussian peak at  $T_0/2$ . This case underpins

the interpretation of SR as a *bona fide* resonance [7]. Note that for the subthreshold bias signal case, one may compute [13], the residence times in the  $A/\sigma \ll 1$  limit (the oft-discussed SR regime). The case of strong (but still *subthreshold*) bias signals and weak noise, i.e.,  $A/\sigma \gg 1$  has recently been analysed in some detail [40]; in this regime, one obtains a near-exponential dependence of  $\langle \Delta T \rangle$  on the asymmetrizing signal  $\epsilon$ , indicating that optimal sensitivity in this technique might be achievable for bias signal amplitudes hovering around the threshold of the energy barrier. Assuming prior knowledge of the sensor characteristics, it is reasonable to expect that one could determine the energy barrier height in practical applications, thereby affording a convenient route to setting the known bias amplitude.

The bias frequency does not figure prominently into the crossing statistics when we work in the non-dynamical limit; however, in the general case, the frequency must be carefully selected. In some ferromagnetic cores, employed for instance in the simple magnetometer used in our experiments, the (non-gaussian) Barkhausen noise floor depends on the bias frequency, through its effect on the slip dynamics of the domain walls; usually there exists a (material-dependent) optimal frequency at which these effects are negligible [30]. Also, for the case of a soft ferromagnetic core the width of the hysteresis loop, which determines the energy dissipated per cycle, can depend on the frequency and amplitude of the bias signal.

Keeping the bias signal amplitude and frequency as low as possible can lead to significantly reduced on-board power; in a real device, this can be an important consideration. However, clearly, the tradeoff between onboard power and the observation time  $T_{ob}$  - which determines the accuracy of the experimental estimate of the quantity  $\langle \Delta T \rangle$  - eventually dictates how the sensor is operated.

The proposed technique is part of the genre of systems operated based on their level crossing dynamics; it should be readily applicable to a large class of dynamic sensors that are operated as detectors of very small target signals, particularly when the detection scheme and the sensor dynamics lend themselves to operation under a known bias signal whose waveform must be carefully selected for optimal sensitivity. In this context we reiterate that the time-sinusoidal bias signal is not necessarily the waveform that yields the best output sensitivity (or resolution); the rigorous analysis of section 6 indicates, in fact, that with the time-sinusoidal bias waveform one might expect the RTD-based approach to yield sensitivity comparable to conventional (PSD-based) techniques. However, we hasten to point out that, while the analysis of section 6 was carried out in the context of a sinusoidal bias waveform, one would usually use a triangular waveform, or the waveform (6) in practice. Both these waveforms outperform the sinusoidal waveform, and they also enable the RTD-based approach to outperform conventional processing as has been observed in experiments (but not shown in this work). In addition,

one must take into account the inherent simplicity of the RTD approach, particularly with regard to the readout electronics and processing. Typically, a simple counting circuit is required, in contrast to the feedback electronics that are usually a part of readout schemes; more complicated electronics usually add more noise to the already present noise-floor. By contrast, in our simple experiments on the prototype nonlinear dynamic sensor (the fluxgate magnetometer) described in the preceding section, one can implement the RTD readout with just one excitation coil and one detection coil without the need for implementing a differential structure (usually done to cancel out steady ambient magnetic fields). Most importantly, the RTD approach can be implemented with low-amplitude and low-frequency bias signals which result in significantly reduced on-board power requirements.

In addition to the experiments described in the preceding section, another laboratory prototype fluxgate magnetometer, using the RTD technique, has already been constructed and operated via the procedure described in this work. It is a planar device, developed in PCB technology, and boasts dimensions small enough to fit comfortably (minus the readout electronics) into a small cigarette pack. The instrument employs a triangular bias waveform and a very simple digital counter to keep track of the crossing events [41]. The laboratory device (excluding the readout electronics) costs about \$1, and has an amorphous metal (or metallic glass alloy, Met-glass) core; current experiments, ongoing at the University of Catnaia, Italy, are aimed at enhancing its sensitivity/resolution by incorporating this device into a coupled array, with the ultimate goal of constructing a network of fluxgates using MeMs technology.

It is worth pointing out that the idea of threshold crossing events leading to a quantification of external signals is deeply rooted in the computational neuroscience repertoire wherein one analyses the response of a single neuron, or even a small network, to a stimulus by examining the statistics of the point process generated by successive threshold crossings or “firings”. This point has already been touched on in section one, but it is important enough to reiterate in this section: our proposed mode of operation actually leads to an implementation of these sensors as “neural”-like devices.

Subsequent work must focus (among other issues) on the determination of the optimal bias signal waveform in terms of specific sensor and operational parameters; clearly, there could be other waveforms besides the sinusoidal bias and the waveform (6) that might be optimal under different conditions. Continued investigations into the (non-gaussian) material-dependent noise floor are also important although, as exploited in this work, this noise may effectively be characterized as gaussian bandlimited noise subject to the appropriate fabrication, materials and geometry constraints.

## IX. ACKNOWLEDGEMENTS

We gratefully acknowledge funding from the Office of Naval Research Code 331. MK, BL, and JR acknowledge funding under the Sweden Armed Forces contract E6706.

---

<sup>†</sup> e-mail: bulsara@spawar.navy.mil

<sup>††</sup> e-mail: seberino@spawar.navy.mil

\* e-mail: luca.gammaitoni@pg.infn.it

\*\* e-mail: mattias.karlsson@foi.se

\*<sup>†</sup> e-mail: bjorn.lundqvist@foi.se

<sup>‡</sup> e-mail: john@foi.se

- [1] See e.g. W. Geyger; *Nonlinear Magnetic Control Devices* (McGraw Hill, New York 1964). P. Ripka; *Sensors and Actuators* **A33**, 129 (1992).
- [2] W. Bornhofft, G. Trenkler in *Sensors, A Comprehensive Survey Vol. 5* eds. W. Gopel, J. Hesse, and J. Zemel (VCH, New York 1989).
- [3] See e.g. A. Barone, and G. Paterno, *Physics and Applications of the Josephson Effect* (J. Wiley, New York, 1982). J. Clarke, *SQUIDS: Theory and Practice*, in *The New Superconducting Electronics*, eds. H. Weinstock and R. Ralston (Kluwer Publishers, Amsterdam 1993).
- [4] See e.g. I. Bunget, M. Prohescu; *Physics of Solid Dielectrics* (Elsevier, NY 1984). D. Damjanovic, P. Muralt, N. Setter; *IEEE Sensors Journal* **1**, 191 (2001).
- [5] See e.g. J. Fraden; *Handbook of Modern Sensors*, and references therein (AIP Press, NY 1997). W. Bornhofft, G. Trenkler in *Sensors, A Comprehensive Survey Vol. 1,2* eds. W. Gopel, J. Hesse, and J. Zemel (VCH, New York 1992).
- [6] For reviews see A. R. Bulsara, L. Gammaitoni, *Physics Today* March p. 39, 1996; L. Gammaitoni, P. Hanggi, P. Jung, F. Marchesoni *Rev. Mod. Phys.* **70**, 225 (1998).
- [7] L. Gammaitoni, F. Marchesoni, S. Santucci; *Phys. Rev. Lett.* **74**, 1052 (1995).
- [8] R. Bartussek, P. Hanggi, P. Jung; *Phys. Rev. E* **49**, 3930 (1994). A. R. Bulsara, M.E. Inchiosa, L. Gammaitoni; *Phys. Rev. Lett.* **77**, 2162 (1996). M. E. Inchiosa, A. R. Bulsara, L. Gammaitoni; *Phys. Rev.* **E55**, 4049 (1997).
- [9] L. Gammaitoni, A. Bulsara; *Phys. Rev. Lett.* **88** 230601 (2002).
- [10] M. Inchiosa, A. Bulsara; *Phys. Rev.* **E53**, R2021 (1996). C. Heneghan, C.C. Chow, J.J. Collins, T.T. Imhoff, S.B. Lowen, M.C. Teich, *Phys. Rev.* **E54**, R2228 (1996). F. Chapeau-Blondeau, *Phys. Rev.* **E55**, 2016 (1997). V. Galdi, V. Pierra, I. Pinto; *Phys. Rev.* **E57**, 6470 (1998). J. Robinson, D. Asraf, A. Bulsara, M. Inchiosa; *Phys. Rev. Lett.* **81**, 2850 (1998). M. Inchiosa, J. Robinson, A. Bulsara; *Phys. Rev. Lett.* **85**, 3369 (2000). S. Kay, *IEEE Sign. Proc. Lett.*, **7**, 8 (2000). I. Goychuk, P. Hänggi, *Phys. Rev.* **E61**, 4272 (2000). J. Robinson, J. Rung, A. Bulsara, M. Inchiosa; *Phys. Rev.* **E63**, 011107 (2001).
- [11] M. Inchiosa, A. Bulsara; *Phys. Rev.* **E58**, 115 (1998).

- [12] L. Gammaitoni, F. Marchesoni, E. Menichella-Saetta, S. Santucci; Phys. Rev. Lett. **62**, 349 (1989).
- [13] T. Zhou, F. Moss, P. Jung; Phys. Rev. **A42**, 3161 (1990). P. Jung; Phys. Rept. **234**, 175 (1993). M. Choi, R. Fox, P. Jung; Phys. Rev. **E57**, 6335 (1998).
- [14] See e.g. H. Tuckwell; *Introduction to Theoretical Neurobiology* (Cambridge Univ. Press, 1988). A. Longtin, A. Bulsara, F. Moss; Phys. Rev. Lett. **67**, 656 (1991). A. Longtin, A. Bulsara, D. Pierson, F. Moss; Biol. Cyb. **70**, 569 (1994). C. Koch, *Biophysics of Computation* (Oxford Univ. Press, NY 1999). A. Longtin, in *Stochastic Dynamics and Pattern Formation in Biological Systems* eds. S. Kim, K.J. Lee and W. Sung (AIP Press, New York 2000).
- [15] See e.g., D. Cox; *Point Processes* (CRC Press, NY 1980). D. Cox, H. Miller; *Stochastic Processes* (Chapman and Hall, London 1996).
- [16] See e.g. G. Papoulis; *Probability, Random Variables, and Stochastic Processes* (McGraw Hill, New York 1991).
- [17] J. Millman, *Microelectronics* (McGraw Hill, New York 1983).
- [18] M. Karlsson, J. Robinson, A. Bulsara, L. Gammaitoni; in Proceedings of the Marine Electromagnetics Meeting (MARELEC), Stockholm, (2001).
- [19] M. Rao, R. Pandit; Phys. Rev. **B43**, 3373 (1991).
- [20] In these units the Curie temperature  $T_c = zJ/k_B$  is set equal to unity;  $z$  is the number of nearest neighbours,  $J$  the strength of the exchange interaction, and  $k_B$  is Boltzmann's constant.
- [21] For a very good overview, see e.g. G. Bertotti; *Hysteresis in Magnetism* (Academic Press, San Diego, 1998).
- [22] See e.g. H. E. Stanley; *Introduction to Phase Transitions and Critical Phenomena* (Oxford Univ. Press, Oxford 1971).
- [23] T. Tome, M. de Oliveira; Phys. Rev. **A41**, 4251 (1990). M. Rao, H. Krishnamurthy, R. Pandit; Phys. Rev. **B42**, 856 (1990). M. Zimmer; Phys. Rev. **E47**, 3950 (1993). B. Chakravarty, M. Acharya; Rev. Mod. Phys. **71**, 847 (1999). H. Fujisaka, H. Tutu, P. Rikvold; Phys. Rev. **E63**, 036109 (2001).
- [24] S. Sides, P. Rikvold, M. Novotny; Phys. Rev. Lett. **81**, 834 (1998). Phys. Rev. **E59**, 2710 (1999).
- [25] Z. Neda; Phys. Rev. **E51**, 5315 (1995). S. Sides, P. Rikvold, M. Novotny; Phys. Rev. **E57**, 6512 (1998). S. Sides; PhD dissertation, Florida State University, 1998.
- [26] W. F. Brown; Phys. Rev. **130**, 1677 (1963).
- [27] T. L. Gilbert; Phys. Rev. **100**, 1243 (1955). L. Landau, E. Lifshitz; *Electrodynamics of Continuous Media* (Pergamon, NY 1960).
- [28] A. Perez-Madrid, J. M. Rubi; Phys. Rev. **E51**, 4159 (1995).
- [29] B. McNamara, K. Wiesenfeld; Phys. Rev. **39**, 4954 (1989).
- [30] J. Deak, A. Miklich, J. Slonczewski, R. Koch; Appl. Phys. Lett. **69**, 1157 (1996). R. Koch, J. Rozen; Appl. Phys. Lett. **78**, 1897 (2001).
- [31] See e.g. C. Gardiner; *Handbook of Stochastic Methods* (Springer Verlag, Berlin 1985).
- [32] L. Gammaitoni, F. Marchesoni, E. Menichella-Saetta, S. Santucci; Phys. Rev. Lett. **62**, 349 (1989). A. Longtin, A. Bulsara, F. Moss; Phys. Rev. Lett. **67**, 676 (1991); Mod. Phys. Lett. **B6**, 1299 (1992). A. Longtin, A. Bulsara, D. Person, F. Moss; Biol. Cyb. **70**, 569 (1994).
- [33] P. Hänggi, P. Jung; Adv. Chem. Phys. **89**, 239 (1995). P. Hänggi, M. Inghiosa, D. Fogliatti, A. Bulsara; Phys. Rev. **E62**, 6155 (2000).
- [34] F. Apostolico, L. Gammaitoni, F. Marchesoni, S. Santucci; Phys. Rev. **E55**, 36 (1997). F. Marchesoni, F. Apostolico, L. Gammaitoni, S. Santucci; Phys. Rev. **E58**, 7079 (1998).
- [35] See e.g. N. Bleistein, R. Handelsman; *Asymptotic Expansions of Integrals* (Dover, NY 1986).
- [36] M. I. Freidlin, A. D. Wentzell; *Random Perturbations of Dynamical Systems* (Springer-Verlag, Berlin 1998).
- [37] T. Cover, J. Tomas; *Elements of Information Theory* (Wiley, New York 1991).
- [38] H.V. Poor; *An Introduction to Signal Detection and Estimation* (Springer-Verlag, Berlin 1988).
- [39] R.S. Liptser, A.N. Shirayev; *Statistics of Random Processes II* (Springer-Verlag, New York 1978).
- [40] A. Nikitin, N. Stocks, A. Bulsara; *Asymmetric Bistable Systems Subject to Periodic and Stochastic Forcing in the Strongly Nonlinear Regime: I. Switching Time Distributions*, Phys. Rev. E, submitted (2002).
- [41] B. Ando, S. Baglio, A. Bulsara, L. Gammaitoni; *Flux-gate Sensors with a Readout Strategy Based on Residence Times Measurements*, IEEE Trans. Magnetics (2002) submitted.